Accepted manuscript (author version)

To appear in:

Iranian Journal of Earth Sciences (Iran J. Earth. Sci.)

E-ISSN: 2228-785X Print ISSN: 2008-8779

Received: 26 December 2024

Revised: 15 April 2025

Accepted: 7 June 2025

DOI: https://doi.org/10.57647/j.ijes.2025.17556

Original Research

Geochemistry and tectonomagmatic setting of the volcanic and Sub-volcanic rocks of the south Gilan, Iranian Alborz mountains: Evidence for Adakite-like and normal arc magmatism

Esmail Ebrahimi nasirmahaleh [1], Mojgan Salavati [1,*], Saeid Hakimi Asiabar[1], Saeed Taki[1]

[1]Department of Geology, La.C., Islamic Azad University, Lahijan, Iran

* Corresponding author: Mojgansalavati@iau.ac.ir

Abstract

As part of the Alborz magmatic zone, Tertiary volcanic and subvolcanic rocks are exposed in southern Gilan province (Rudbar and Rostamabad) and have been evaluated for the first time in this study. Field and petrographic studies indicate a compositional spectrum from basalt, andesite to trachyandesite, dacite to trachy-dacite, rhyodacite. Geochemically, the rocks were divided into two distinct groups: adakitic rocks with high Sr, Sr/Y and La/Yb and low MgO, Y and Yb, and typical calc-alkaline rocks of arc nature. All rocks show a parallel enrichment trend from LREE to HREE. Both partial melting and crystal fractionation play important role in controlling the compositional diversity and composition of the main magma of the samples. Both rock groups formed in a subduction zone environment and were produced with different degrees of melting in a slab window environment. All data indicate that the rocks were formed during the subduction to the south of the Para-Tethys oceanic crust. A "ridge-trench" model for the tectonomagmatic scenario has been proposed, suggesting that these lavas were formed in a Para-Tethys supersubduction zone. According to this model, a slab window was formed after the subduction of the Para-Tethys oceanic crust. Partial melting of this crust at depth, with different degrees of partial melting in some areas, coinciding with the formation of a tectonic window in the subduction zone, led to the production of adakitic magma. Typical arc rocks with higher degrees of melting and at shallower depths formed further away from the subduction zone.

Keywords: Adakite, Slab window, A arc magmatism, Para-Tethys, Gilan, Iran

1. Introduction

Iran, as a microcontinent, is part of the Alpine-Himalayan orogenic belt, with extensive magmatic (volcanic and intrusive) activities, especially during the Cenozoic. Most of the volcanic activities in Iran are associated with the subduction of the Neo-Tethys Ocean and its branches (Berberian and King, 1981; Jung et al., 1976; Berberian et al., 1982; Axen et al., 2001; Shahabpour, 2007; Asiabanha et al., 2009; Mollai et al., 2021). These volcanic activities have been reported in two main volcanic zones: the Alborz zone in northern Iran and the Urumieh-Dokhtar zone surrounding the central Iranian microcontinent (Jung et al., 1976; Berberian et al., 1982; Shahabpour, 2007; Ghasemi and Talbot, 2005; Asiabanha et al., 2009; Bahajroy and Taki, 2014; Ousta et al., 2024; Elmi et al., 2025).

In the Alborz zone, several magmatic activities occurred during and after the Eocene and continue to the present day (Asiabanha et al., 2012). Some studies have attributed the formation of volcanic rocks in this region to the northward subduction of the Neo-Tethys Ocean beneath north-central Iran (Teimouri et al., 2018; Berberian and King, 1981; Golonka, 2004; Asiabanha et al., 2009; Asiabanha and Bardintzeff, 2014; Dabiri et al., 2018) and believe that this subduction led to magmatism in a continental arc setting (Kalantari et al., 2008; Valizadeh et al., 2008; Abdolahadi et al., 2025) or, instead, in a back-arc basin extension (BAB) setting (Asiabanha et al., 2012; Salehpour et al., 2025). Recent studies have shown that Cenozoic igneous activity in the northern Alborz in Gilan Province (south of the Caspian Sea) was generated by southward subduction of Para-Tethys oceanic crust (as a result of a local ocean) beneath the Alborz (Rezania ye Komachaly et al., 2021; Eyuboglu et al., 2012; Rezania ye Komachaly et al., 2022; Salavati et al., 2013; Salavati et al., 2009; Talebian Borojenie et al., 2025). Thus, the Alborz Mountains in northern Iran are confined between two subductions.

In the study area, there are no sufficient geochemical and geochronological data for the volcanic rocks of the Northern Alborz in southern Guilan Province. The present study (with new geological, petrological and geochemical data that have not been reported before) attempts to provide new reasons and evidence to determine the geodynamic evolution of the Northern Alborz in the study area.

2. Geological setting

The study area is part of the Rudbar 1:100,000 geological map (Nazari and Salamati, 1998) (Fig. 1), according to structural classifications, belongs to the Gorgan-Rasht zone and the Caspian Sea subduction system (Eftekhar Nejad, 1980). The area is also associated with Eocene magmatism in the Alborz orogenic belt.

The Alborz Eocene volcanic complex (Karaj Formation) consists of two primary facies (Asiabanha et al., 2009):

1. Volcanic-sedimentary facies and 2. Mafic-felsic subaerial lava flows.

The dominant geological units in the study area include Paleozoic, Mesozoic, and Cenozoic stratigraphic Formations.

The oldest rocks, which belong to the Paleozoic, consist of red to gray arkosic sandstones with a quartzite bases, interbedded shales, and dark gray, thick chert limestones. The Cenozoic section begins with detrital conglomerates from the Upper Cretaceous to the Paleocene and continues with volcanic activity, such as tuff deposition and lava flows during the Eocene. The volcanic activity during the Upper Eocene becomes increasingly acidic, transitioning to intermediate and basic lavas during the Miocene. The volcanic sequence, as shown on the Rudbar geological map, transitions from south to north, with younger units containing andesite, dacite, rhyodacite, and tuffs (Nazari and Salamati, 1998; Ghasempour et al., 2014; Khosaravi et al., 2020). In the study area, almost all igneous rocks are of Paleogene age. Based on field studies, the Eocene volcanic sequence consists of lavas and pyroclastic rocks. The oldest igneous units (E^{at}) are gray to red andesitic and dacitic tuffs associated with sandstone and conglomerate interlayers, visible as a small outcrop in the eastern of the area. The tuffs of this unit are mostly of dacite or andesite composition. On both sides of the Sefid Rud River, a small outcrop of green to gray rhyodacite tuff layers, sometimes interlayering with iron ore layers (Et), is visible. Lavas with megaporphyritic texture are introduced as the E^{tv} unit, and in hand samples, the rocks of this unit are characterized by coarse plagioclase crystals. Most of the study area is covered by the basic to intermediate volcanic lava unit ($E^{tv}{}_3$). The (adakite) rocks form the intermediate to acidic volcanic units of the $E^{tv}{}_2$ unit that exposed in the central and southern part of the area as dacitic, rhyodacitic and rhyolite lavas. The youngest volcanic units area in the north of the area include basaltic dacitic and rhyodacitic lavas.

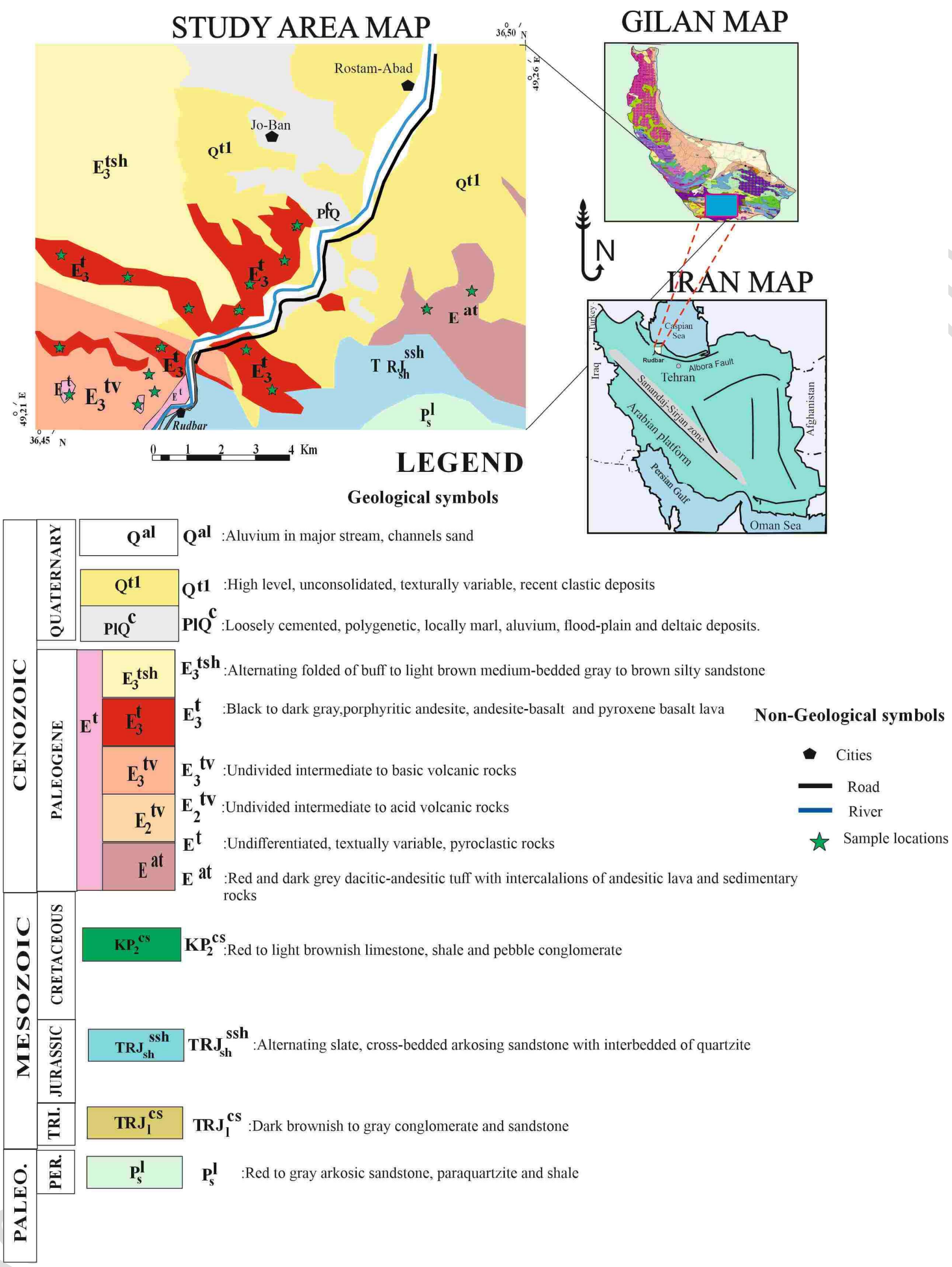

Figure 1. Geological map of the studied area (after Rudbar (Nazari and Salamati, 1998).

3. Methods and techniques

Based on field observations and lithology, 60 rock samples were collected from different parts of the area for laboratory study. Petrographic studies were performed on all samples to determine mineral type and textural relations. Then, based on the petrographic observations, 30 samples were selected for geochemical analysis.

For geochemical analysis, the selected samples were crushed and prepared using carbide mills and were analyzed in Activation Laboratories (Act Lab) in Canada.

Inductively coupled plasma atomic emission spectrometry (ICP-AES) and inductively coupled plasma mass spectrometry (ICP-MS) were used to measure concentrations of major and trace elements. These techniques provide high-precision data on the elemental composition of the samples, which is essential for understanding the genesis and evolution of the samples. The geochemical results are presented in Tables 1 and 2 for the sample groups. Finally, a robust framework for interpreting the petrogenesis and tectonic setting of the volcanic and sub-volcanic rocks of the region was presented by combining field observations, petrographic and geochemical analyses.

Table 1. Representative major oxide and trace element data of the Normal calc-alkaline samples by ICP-AES and ICP-MS (major and elements are given in wt. % and ppm, respectively). Fe_2O_3 represents total iron oxide as ferric iron, LOI= Lost on ignition

Sample No.	**Ro-9**	**Ro-7**	**Ro-8**	**Ro-6**	**Ro-14**	**Ro-11**	**Ro-10**	**Ro-107**	**Ro-108**	**Ro-109**	**Ro-110**	**Ro-110**	**Ro-106**	**Ro_108_1**	**Ro_112_2**	**Ro-162**	**Ro-15**
SiO_2	55.60	52.90	53.10	58.30	51.50	60.60	57.50	59.10	59.90	58.10	51.00	65.70	64.80	52.50	54.50	49.80	50.40
Al_2O_3	18.70	18.60	17.70	17.60	16.40	15.10	15.20	16.20	16.20	16.90	16.80	15.80	16.30	16.50	15.00	17.40	17.60
Fe_2O_3 (T)	6.60	8.60	8.80	6.40	9.80	5.50	5.10	6.80	6.60	6.50	10.60	4.10	4.70	8.30	7.40	8.90	8.90
MnO	0.23	0.16	0.15	0.13	0.20	0.07	0.09	0.13	0.11	0.12	0.16	0.10	0.06	0.12	0.12	0.11	0.17
MgO	2.73	3.37	3.70	2.28	5.92	1.78	2.90	2.38	2.26	2.65	5.03	1.18	1.00	3.99	5.00	1.48	2.26
CaO	5.76	8.25	8.03	5.22	8.88	4.61	5.54	5.44	5.69	5.18	8.77	3.48	1.52	8.15	7.25	9.55	7.96
Na_2O	4.11	3.25	3.24	4.58	2.63	3.78	3.38	3.29	3.24	3.74	3.01	4.35	4.19	2.94	2.75	3.47	3.84
K_2O	1.95	1.87	1.60	2.80	1.97	4.04	4.06	4.06	3.99	3.24	1.36	2.55	4.09	3.18	4.08	3.40	2.97
TiO_2	0.89	1.01	1.02	0.87	1.04	0.88	0.82	0.90	0.87	0.91	1.42	0.46	0.55	1.07	0.90	1.20	1.22
P_2O_5	0.34	0.28	0.28	0.26	0.31	0.48	0.43	0.30	0.31	0.32	0.24	0.16	0.20	0.42	0.33	0.58	0.56
LOI	3.90	1.95	1.93	2.17	2.10	4.04	4.15	2.26	1.86	3.18	1.64	2.41	3.21	2.03	1.91	5.17	3.66
Total	100.84	100.37	99.64	100.63	100.80	100.98	99.22	100.94	100.99	100.89	100.07	100.24	100.71	99.21	99.31	100.97	99.56
Sc	16.00	24.00	24.00	19.00	33.00	10.00	10.00	16.00	16.00	15.00	29.00	5.00	8.00	22.00	19.00	13.00	14.00
Be	2.00	1.00	2.00	2.00	2.00	3.00	3.00	3.00	2.00	3.00	1.00	2.00	3.00	3.00	3.00	3.00	3.00

V	158.00	234.00	232.00	179.00	273.00	79.00	79.00	157.00	149.00	122.00	298.00	45.00	53.00	223.00	166.00	190.00	179.00
Ba	623.00	578.00	476.00	667.00	422.00	890.00	817.00	796.00	802.00	808.00	397.00	648.00	647.00	598.00	1058.00	583.00	495.00
Sr	579.00	728.00	558.00	482.00	603.00	462.00	938.00	460.00	431.00	436.00	521.00	350.00	256.00	512.00	579.00	608.00	816.00
Y	23.00	22.00	23.00	21.00	21.00	22.00	21.00	26.00	25.00	30.00	21.00	18.00	16.00	22.00	21.00	23.00	23.00
Zr	110.00	78.00	100.00	136.00	91.00	199.00	189.00	207.00	198.00	258.00	83.00	187.00	235.00	154.00	177.00	182.00	195.00
Cr	< 20	< 20	< 20	< 20	80.00	40.00	40.00	30.00	30.00	20.00	40.00	< 20	80.00	100.00	190.00	30.00	30.00
Co	16.00	23.00	23.00	16.00	28.00	14.00	15.00	14.00	15.00	13.00	28.00	5.00	9.00	26.00	25.00	22.00	25.00
Ni	< 20	< 20	< 20	< 20	30.00	40.00	40.00	< 20	< 20	< 20	< 20	< 20	< 20	50.00	80.00	< 20	20.00
Cu	130.00	110.00	90.00	50.00	40.00	60.00	60.00	60.00	80.00	60.00	60.00	100.00	70.00	120.00	90.00	40.00	50.00
Zn	120.00	90.00	80.00	70.00	90.00	60.00	70.00	80.00	70.00	90.00	80.00	60.00	50.00	80.00	80.00	90.00	80.00
Ga	20.00	19.00	19.00	19.00	17.00	20.00	22.00	19.00	18.00	22.00	21.00	18.00	18.00	18.00	19.00	15.00	18.00
Ge	1.00	2.00	2.00	2.00	2.00	1.00	1.00	2.00	2.00	2.00	2.00	1.00	1.00	2.00	2.00	3.00	2.00
As	9.00	28.00	6.00	11.00	< 5	10.00	9.00	10.00	< 5	< 5	11.00	< 5	< 5	19.00	54.00	< 5	< 5
Rb	36.00	31.00	30.00	74.00	44.00	132.00	144.00	127.00	122.00	123.00	31.00	79.00	115.00	91.00	147.00	88.00	73.00
Nb	6.00	4.00	7.00	7.00	6.00	20.00	19.00	20.00	18.00	23.00	7.00	14.00	25.00	9.00	12.00	16.00	17.00
Cs	4.30	1.00	0.50	3.10	0.50	2.80	2.20	2.40	1.90	3.40	0.70	1.70	1.70	0.70	7.70	< 0.5	0.60
La	23.90	18.40	20.10	26.90	18.90	50.00	52.80	32.40	30.10	42.10	17.60	33.70	41.60	28.10	39.40	35.70	37.80
Ce	48.80	39.00	40.50	52.30	38.80	99.00	98.90	62.60	58.80	79.80	36.40	61.80	72.80	54.20	74.80	67.50	72.30
Pr	5.75	4.70	4.98	5.69	4.73	11.40	11.40	7.29	6.95	9.48	4.69	6.14	7.10	6.56	8.37	7.52	7.98
Nd	25.00	20.60	20.60	22.90	20.30	41.50	41.10	28.70	26.90	35.50	19.90	22.00	25.30	25.80	31.90	29.70	30.40
Sm	5.20	4.70	5.10	4.80	4.60	7.30	7.30	5.90	5.40	7.00	4.50	3.90	4.30	5.50	6.30	5.90	6.20
Eu	1.55	1.49	1.38	1.26	1.38	1.58	1.59	1.39	1.34	1.67	1.39	1.03	1.05	1.55	1.49	1.79	1.81
Gd	4.50	4.20	4.70	3.90	4.20	5.00	5.00	4.70	4.60	5.90	4.10	3.10	3.10	4.80	5.30	5.00	4.90
Tb	0.70	0.70	0.70	0.60	0.70	0.70	0.70	0.80	0.70	0.90	0.70	0.50	0.50	0.80	0.80	0.80	0.80
Dy	4.20	4.10	4.60	3.80	4.20	3.90	4.00	4.70	4.50	5.50	4.00	3.10	3.00	4.40	4.50	4.40	4.60

Ho	0.80	0.80	0.90	0.80	0.80	0.80	0.80	0.90	0.90	1.00	0.80	0.60	0.60	0.90	0.90	0.90	0.90
Er	2.40	2.40	2.70	2.10	2.40	2.20	2.20	2.60	2.60	2.90	2.20	1.90	1.80	2.40	2.40	2.40	2.50
Tm	0.35	0.35	0.42	0.31	0.34	0.34	0.36	0.44	0.43	0.48	0.33	0.29	0.27	0.40	0.38	0.35	0.36
Yb	2.20	2.20	2.90	2.20	2.10	2.20	2.30	2.80	2.70	3.10	2.10	2.00	1.80	2.50	2.40	2.30	2.30
Lu	0.37	0.36	0.49	0.38	0.36	0.34	0.31	0.41	0.40	0.47	0.31	0.34	0.30	0.35	0.33	0.36	0.37
Hf	2.70	2.00	2.80	3.30	2.40	5.70	5.30	5.30	5.10	6.40	2.40	4.10	4.70	3.60	4.50	3.70	4.00
Ta	0.30	0.20	0.40	0.50	0.30	1.10	1.10	1.10	0.90	1.30	0.30	1.20	2.20	0.90	1.10	0.90	0.90
Pb	13.00	6.00	5.00	12.00	8.00	19.00	15.00	19.00	12.00	34.00	< 5	9.00	9.00	7.00	24.00	6.00	6.00
Th	3.80	2.50	3.20	7.80	3.30	19.70	18.30	10.70	10.20	14.10	3.60	11.80	10.30	6.50	13.30	5.00	5.20
U	1.30	0.80	1.10	2.30	1.00	4.90	5.60	3.30	3.10	4.20	1.10	3.50	2.50	2.20	3.90	2.00	1.80
K_2O/ Na_2O	0.47	0.58	0.49	0.61	0.75	1.07	1.20	1.23	1.23	0.87	0.45	0.59	0.98	1.08	1.48	0.98	0.77
Sr/Y	25.17	33.09	24.26	22.95	28.71	21.00	44.67	17.69	17.24	14.53	24.81	19.44	16.00	23.27	27.57	26.43	35.48
La/Yb	10.86	8.36	6.93	12.23	9.00	22.73	22.96	11.57	11.15	13.58	8.38	16.85	23.11	11.24	16.42	15.52	16.43
Nb/Zr	0.05	0.05	0.07	0.05	0.07	0.10	0.10	0.10	0.09	0.09	0.08	0.07	0.11	0.06	0.07	0.09	0.09
Th/Ce	0.08	0.06	0.08	0.15	0.09	0.20	0.19	0.17	0.17	0.18	0.10	0.19	0.14	0.12	0.18	0.07	0.07
Sr/Ce	11.86	18.67	13.78	9.22	15.54	4.67	9.48	7.35	7.33	5.46	14.31	5.66	3.52	9.45	7.74	9.01	11.29

Table 2. Representative major oxide and trace element data of the adakitic samples by ICP-AES and ICP-MS (major and elements are given in wt. % and ppm, respectively). Fe_2O_3 represents total iron oxide as ferric iron, LOI= Lost on ignition

Sample No.	**MA11**	**MA1**	**MA12**	**MA10**	**MA13**	**MA15**	**MA16**	**MA18**	**MA20**	**MA17**	**MA21**	**MA22**	**MA23**
SiO_2	63.1	62.6	66.4	67.1	66.5	65.2	62.9	63.6	61.9	65.2	64.5	61.9	62.8
Al_2O_3	15.2	15.2	15.9	15.9	15.8	15.2	15.3	15.7	15.2	15.3	15.8	15.3	15.1
$Fe_2O_{3(t)}$	4.5	4.6	3.9	3.9	3.9	4.5	4.4	4.3	4.2	3.8	4.1	4.4	4.1
MnO	0.05	0.08	0.05	0.07	0.05	0.06	0.05	0.06	0.05	0.06	0.05	0.05	0.05
MgO	2.02	2.01	0.71	1.1	0.9	2.3	2.1	2.2	2.8	2.12	2.28	2.02	2.6
CaO	3.9	3.9	3.3	3.2	3.1	3.9	3.6	3.8	3.6	3.9	3.8	3.9	3.5
Na_2O	2.8	2.9	3.9	3.8	3.8	2.9	2.9	2.9	3.1	3.9	3.4	3.8	3.8
K_2O	2.9	2.8	4.1	4	3.9	3.1	3.7	3.5	3.8	4	3.6	3.6	3.1

TiO_2	0.49	0.49	0.44	0.49	0.46	0.41	0.42	0.43	0.46	0.44	0.45	0.44	0.46
P_2O_5	0.12	0.11	0.17	0.19	0.16	0.15	0.17	0.19	0.14	0.18	0.19	0.15	0.15
LOI	5.2	5.3	1.5	1.1	1	2.1	3.5	3.8	3.4	1.5	2	3.5	3.5
Total	100.4	99.9	100.5	100.9	99.6	99.8	99.2	100.6	98.8	100.5	100.2	99.3	99.3
Sc	7	8	6	7	6	8	7	6	8	7	9	7	7
Be	2	2	2	2	2	2	2	2	2	2	2	2	2
V	85	86	71	70	72	84	87	85	79	74	76	86	81
Ba	972	970	791	790	788	969	975	975	984	798	784	975	980
Sr	1881	1882	455	450	454	1880	1879	1884	1887	540	565	1881	1883
Y	14	14	13	12	14	14	14	13	11	10	12	13	13
Zr	15	151	173	171	170	152	152	155	157	17	173	150	155
Co	9	9	6	5	6	8	9	8	6	7	9	8	8
Cu	6	6	30	35	40	60	55	45	40	60	50	60	55
Zn	80	90	40	41	40	90	80	90	100	90	80	80	100
Ga	16	17	16	18	17	15	16	18	17	19	17	16	16
Ge	1	1	1	1	1	1	1	1	1	1	1	1	1
As	6	5	8	5	7	6	8	6	5	7	6	5	6
Rb	80	81	85	89	84	82	91	89	85	81	83	80	88
Nb	9	9	10	11	9	8	8	9	10	8	7	9	11
Cs	4.8	4.9	2.5	2.2	2.4	4.7	4.7	4.9	4.8	2.4	2.3	4.9	4.8
La	26.7	26.8	29.8	29.6	29.4	27.3	26.4	26.9	26.8	29.2	29.1	26.8	26.8
Ce	47.9	48.2	52	53	51	51	50.1	47.9	48.1	50.1	52.6	48.2	47.7
Pr	4.87	4.88	5.29	5.18	4.9	4.78	5.12	5.32	4.85	4.78	4.9	4.88	4.9
Nd	18.4	18.7	19.1	19.3	18.98	18.8	18.7	18.6	18.7	18.9	19.2	18.7	18.9
Sm	3.2	3.3	3.3	3.4	3.1	3.5	3.2	3.1	3.1	3.3	3.2	3.3	3.3
Eu	0.99	0.99	0.95	0.94	0.96	0.98	0.97	0.96	0.99	0.98	0.97	0.99	0.95
Gd	2.4	2.5	2.7	2.6	2.4	2.8	2.8	2.4	2.8	2.6	2.7	2.5	2.8
Tb	0.4	0.4	0.4	0.4	0.4	0.4	0.4	0.4	0.4	0.4	0.4	0.4	0.4
Dy	2.6	2.5	2.5	2.7	2.6	2.5	2.4	2.7	2.6	2.5	2.4	2.5	2.6
Ho	0.5	0.5	0.5	0.5	0.5	0.5	0.5	0.5	0.5	0.5	0.5	0.5	0.5
Er	2.1	1.6	1.5	1.4	1.6	1.9	1.9	1.6	1.7	1.9	1.8	1.6	1.7
Tm	0.23	0.23	0.23	0.23	0.22	0.23	0.35	0.33	0.24	0.25	0.35	0.23	0.24

Yb	1.5	1.6	1.5	1.4	1.5	1.6	1.5	1.6	1.7	1.5	1.6	1.6	1.6
Lu	0.28	0.27	0.27	0.25	0.29	0.28	0.28	0.29	0.26	0.24	0.29	0.27	0.28
Hf	3.5	3.4	4	3.8	4.2	3.6	3.5	3.3	3.4	3.9	3.7	3.4	3.6
Ta	0.7	0.7	0.8	0.7	0.9	0.7	0.8	0.9	0.7	0.6	0.9	0.7	0.8
Pb	10	10	21	20	23	11	12	18	17	20	22	10	17
Th	8.1	7.9	8.9	8.5	8.6	8.2	8.2	8.1	8.4	8.3	8.1	7.9	8.2
U	2.6	2.7	2.8	2.7	2.6	2.8	2.7	2.6	2.4	2.9	2.8	2.7	2.4
K_2O/ Na_2O	1.05	0.98	1.06	1.06	1.03	1.07	1.27	1.19	1.23	1.05	1.04	0.94	0.83
Sr/Y	134.36	134.43	35	37.5	32.43	134.29	134.21	144.92	171.55	54	47.08	144.69	144.85
La/Yb	17.8	16.75	19.87	21.14	19.6	17.06	17.6	16.81	15.76	19.47	18.19	16.75	16.75
Nb/Zr	0.6	0.06	0.06	0.06	0.05	0.05	0.05	0.06	0.06	0.47	0.04	0.06	0.07
Th/Ce	0.17	0.16	0.17	0.16	0.17	0.16	0.16	0.17	0.17	0.17	0.15	0.16	0.17
Sr/Ce	39.27	39.05	8.75	8.49	8.9	36.86	37.5	39.33	39.23	10.78	10.74	39.02	39.48

4. Petrography

The Paleogene volcanic and sub-volcanic rocks of the area exhibit a compositional range from basic (basalt) to felsic (dacite to rarely rhyolite). These rocks have predominantly display porphyritic textures, characterized by abundant plagioclase phenocrysts set within a fine-grained or glassy groundmass. The petrographic characteristics of each rock type are described below:

4.1. Basalts

Porphyry basalts have microlitic or glassy groundmass and glomeroporphyry are the main mafic rocks in the region. Clinopyroxene, plagioclase and sometimes olivine are the major minerals. They occur as phenocrysts, microphenocrysts and small crystals (Fig. 2a, b, c). Clinopyroxenes are phenocrysts and microcrystals that sometimes occur with glomeroporphyritic aggregates and often have a reaction rim around them, due to mineral reaction with magma (Fig. 2d, e). Some clinopyroxene phenocrysts show simple, repetitive twinning (Fig. 2b, c, i), spongy textures (Fig. 2f, g) or homogeneous spongy textures (Fig. 2h, i) or reaction rims, indicating mineral interaction with the magma. Symmetrical extinction is also observed in some clinopyroxene phenocrysts (Fig. 3a). Olivine crystals are often altered to iron oxides or chlorite, and some are completely unaltered, with only their mold remaining (Fig. 3b). Plagioclase crystals often show sieve texture and zoning (Fig. 2h, 4b, c). Minor phase minerals include altered apatite and chlorite, calcite, and opacity. Olivine and pyroxene phenocrysts make up about 15-20% of the rock volume.

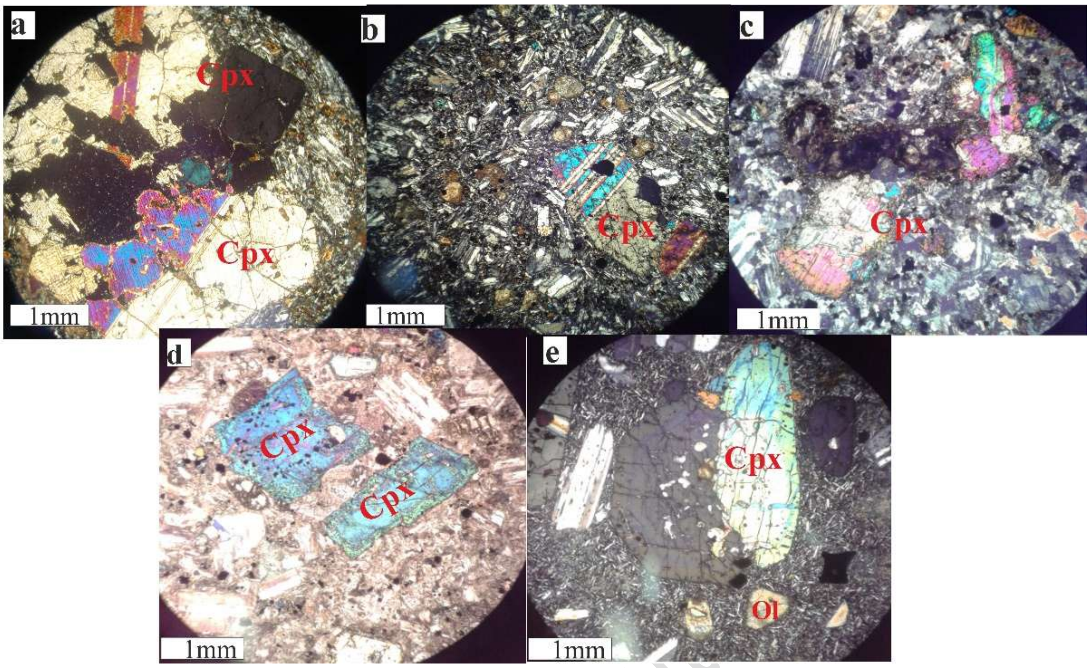

Figure 2. Petrographic image of basalts sample: a) Clinopyroxene, plagioclase, and olivine with glomeroporphyritic texture, clinopyroxene have repetitive twinning, b) Porphyritic texture with clinopyroxene phenocryst (with repetitive twinning), c) Reaction rim around the clinopyroxene phenocryst, d) Clinopyroxene phenocryst with spongy texture in rims and clean cores, e) Spongy texture in clinopyroxene phenocryst cores, and sieve texture in plagioclase and altered olivine. (All in XPL light) Abbreviations from Whitney and Evans (2010).

4.2. Basaltic andesites, andesitic basalt

This group occurs as lava flows with lava layering. The basaltic andesite lavas consist of an assemblage of plagioclase, olivine, pyroxene, and magnetite that exhibit porphyritic, hyaloporphyric with glassy matrix, microlithic porphyritic, and glomeroporphyritic textures (Fig. 3 d, e). Plagioclase and clinopyroxene represent both phenocrysts and fine-grained matrix (in andesitic basalts clinopyroxenes are more plagioclase while andesitic basalts is opposite). The main difference between, the two groups, basaltic andesites, and olivine basalts, is the absence of olivine as a major phenocryst phase in basaltic andesite rocks. Plagioclases often show distinct dusty and sieve texture, both in the rim and in the core of the crystals. Sometimes clinopyroxene phenocrysts show reaction rims (Fig. 3 d). Ground mass accounts for 65% of the rock's volume.

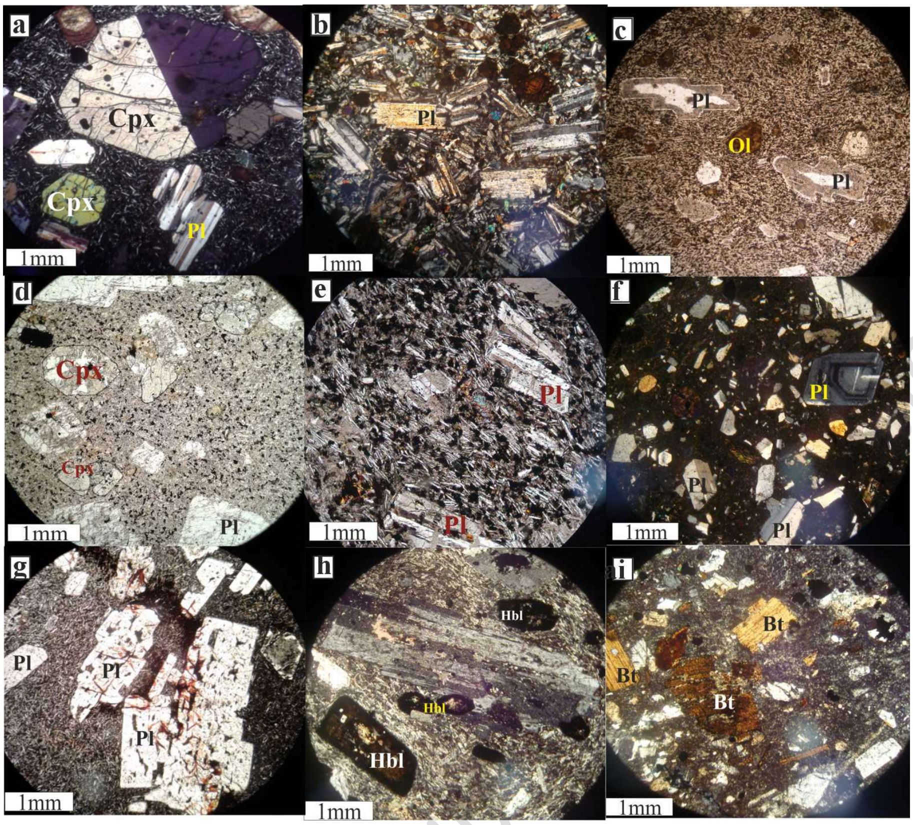

Figure 3. Photomicrographs of thin sections of a) Clinopyroxene phenocryst with symmetrical extinction and porphyritic texture in basalt, (XPL light); b) Phenocrysts of Plagioclase with sieved texture, and iddingsitized olivine in basalt, (XPL light); c) Dusty texture in rim or core of plagioclase phenocryst and altered olivine in basalt, (PPL light); d) Reaction rim around the phenocryst of clinopyroxene in basaltic andesite, (PPL light); e) Microlitic porphyritic texture in andesitic basalt, and sieved plagioclase phenocryst, (XPL light); f) Hyaloporphiritic texture and oscillatory zoning in andesite, (XPL light); g) Sieve texture of the coarse-scale in andesite, (XPL light); h) porphyromicrolitic texture and opacitic rim in amphibole phenocrysts in andesites, (XPL light); I) Biotite phenocrysts in andesite, (XPL light); Abbreviations from Whitney and Evans (2010).

4.3. Andesite

Andesite and pyroxene andesite lavas exhibit microgranular porphyritic or microlithic textures with glassy groundmasses. These rocks are rich in plagioclase, clinopyroxene, and opaque oxides, occasionally accompanied by amphibole and biotite (Fig. 3f). The difference between these rocks and the previous groups is the occurrence of amphibole minerals (aqueous phase) in them. These minerals show a wide range in size from microphenocrysts to megacrysts (seriate texture). Plagioclases such as phenocrysts and microcrystals are the main and abundant minerals of these rocks. Plagioclase occurs as euhedral to subhedral prismatic to tabular crystals and is medium to coarse grained. Zoning and sieve texture are found in present plagioclase crystals (Fig. 3f, g). Pyroxene are the third most abundant crystal in this rock group. In andesites, compared to pyroxene andesites, clinopyroxene crystals are reduced and only occasionally occur as phenocrysts. Amphibole has generally has a rim of opacity. The thickness of the opacity rim in amphibole, in the andesitic samples is greater than that of those in the pyroxene andesites. Sometimes an amphibole crystal is completely covered with by an opacity rim (Fig. 3 h). Phenocrysts of biotite are also observed in the andesites (Fig. 3 i). The presence of biotite phenocrysts with opacitic rims is a distinguishing feature of the andesites. In andesitic rocks, opaque minerals are secondary minerals and apatites are accessory minerals.

4.4. Trachyandesites and Trachytes

Trachyandesitic rocks represent a variety of porphyritic, flow, glomero-porphyritic, and sieve textures. Plagioclase, amphibole, and clinopyroxene are the major phenocrysts in trachyandesite while amphibole, biotite, and alkali feldspar with porphyritic textures are phenocrysts in the trachyte. In trachyandesitic rocks, plagioclase is 65-75 vol%, and phenocrysts of that show zoning and sieve texture at the crystal margins of the crystal. Some plagioclase crystals are decomposed into sericite, chlorite, and clay minerals. Secondary quartz is often observed as fine grains in the matrix or as a filler in fractures. Amphiboles (with 3-7 vol%) have an opacitic rim (Fig. 4 a), or in some crystals have decayed from the rim (Fig. 4 b). Biotite in trachyte forms subhedral to resorbed phenocrysts. Opacity rim and fine-grained decomposition products are found around biotite crystals (Fig. 4 c).

4.5. Dacite and Rhyodacite

These felsic rocks are typically observed as thick lava flows or, rarely, as lava domes. They exhibit a variety of textures, including porphyritic, hyaloporphyritic, felsitic, and microfelsitic. The mineral assemblage includes plagioclase, alkali feldspar, amphibole, biotite, quartz, and opaque oxides (Fig. 4 d, f, h, i). Alkali feldspar phenocrysts occasionally show perthitic textures, while biotite is often altered to opaque minerals (Fig. 4 d, e, i). Biotite shows an opacitic rim or is altered to opaque minerals (Fig. 4 f). Quartz phenocrysts sometimes show corrosion gulfs.

In rhyodacites, quartz phenocrysts sometimes have corrosion gulfs (Fig. 4 h). Petrographic observations show the presence of crystal fractionation in the samples. This fractionation of basaltic magmas started with the separation of olivine phenocrysts. During the progression of the fractionation process, the amount of plagioclase and pyroxene increased in basaltic andesite. With the continuation of the process, the amount of water in the magma increased, and amphibole and biotite appeared. In the end, mafic minerals were removed, and quartz and alkali feldspar appeared in felsic magma, mafic minerals were removed and quartz and alkali feldspar appeared in felsic magma. There are two texture groups in all rock groups: A) texture related to crystalline growth, including sieve texture and zoning, and b) morphological textures, such as glomerular crystals and microlites, which are formed under the influence of dynamic processes during magma crystallization, such as convection, outgassing, or explosive eruptions. The heterogeneous compositions of plagioclase in rims and cores, dusty or sifted plagioclase, pseudomorphs after mafic phases on amphibole and biotite (Fig. 4 e, f), and reaction rims on clinopyroxene (Fig. 4f) are evidence of varying degrees of disequilibrium features in the volcanic rocks. In all rock groups, microtextures such as sieve textures, zoning, and glomeroporphyritic structures are common, reflecting dynamic processes during magma crystallization. Disequilibrium features, including oscillatory zoning, crystal dissolution, and corrosion, indicate magmatic contamination and assimilation.

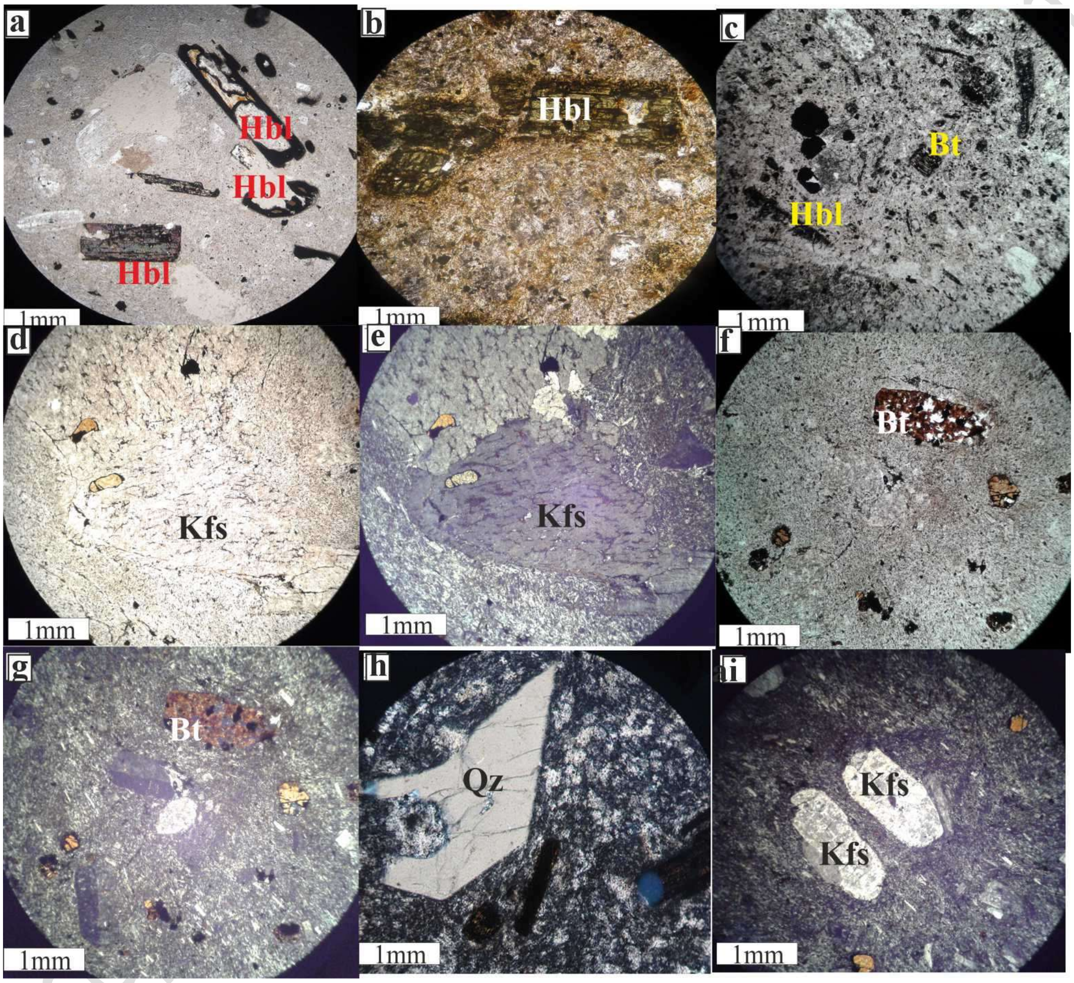

Figure 4. Photomicrographs of thin sections of a) Hornblend with opacitised rim in trachyandesites, (XPL light); b) Decayed rim in hornblende in trachyandesites, (XPL light); c) Opaque rims and fine-grained breakdown products around of biotite and opacitised hornblende in trachytes, (XPL light); d, e) Alkali feldspar phenocryst with Perthitic texture in dacite, (d: PPL light; and E: XPL light); f, g) Altered biotite in dacite, (f: PPL light; and g: XPL light); h) Corrosion gulf in quartz phenocryst in rhyodacite, (XPL light); i) porphyromicrolitic texture with phenocrysts of alkali feldspar in rhyodacite, (XPL light); Abbreviations from Whitney and Evans (2010).

5. Geochemistry

The geochemical characteristics of the studied rocks reveal two distinct groups:

1. Adakite and adakite-like rocks (**Fig.** 7): These are characterized by high Sr, Sr/Y, and La/Yb values, low MgO, Y, and Yb contents, enrichment in light rare earth elements (LREEs) and large ion lithophile elements (LILEs), and depletion in heavy rare earth elements (HREEs), Nb, and Ti. These rocks lack a negative europium anomaly which is consistent with the characteristics of adakitic or adakite-like rocks.

2. Normal calc-alkaline rocks: These exhibit geochemical characteristics typical of ordinary calc-alkaline volcanic rocks.

Adakitic Rocks

Adakitic samples have SiO_2 contents ranging from 61.87 to 67.1 wt. %, low TiO_2 (0.41–0.49 wt. %), moderate Al_2O_3 (15.12–15.97 wt. %), and low CaO (0.93–1.3 wt. %) and MgO (0.7–2.8 wt. %) contents. These rocks are also enriched in Ba (784–980 ppm), Sr (450–1883 ppm), and Zr (150–173 ppm), while depleted in Nb (7–11 ppm) and of Fe_2O_3tot values between 4.56 to 10.6 wt. %. Additionally, they exhibit high alkali content (Na_2O: 2.88–3.87 wt. %; K_2O: 3.9–4.1 wt. %) and high K_2O/Na_2O ratios (0.83–1.27), which is very similar to the properties of the adakites as described by Castillo (2012) and consistent with subduction-derived adakites (Dokuz et al., 2013; He et al., 2020).

Normal Calc-alkaline Rocks

The normal calc-alkaline samples have a range of SiO_2 contents between (49.76–65.72 wt%) and low TiO_2 (0.46–1.42 wt%), CaO (1.52–9.55 wt%), and MgO (1–5.92 wt%). These rocks are also enriched in Al_2O_3 (15.14–18.69 wt%) and alkalis (Na_2O: 2.75–4.58 wt%) with Fe_2O_{3tot} values ranging from 4.06 to 10.6 wt%. Trace element analysis shows Ba (394–1058 ppm), Sr (256–938 ppm), Zr (78–258 ppm), and Nb (4–25 ppm), 17.6 ppm < La < 50 ppm, 16 ppm<Y < 30 ppm. They display moderate enrichment in LREEs relative to HREEs and a positive slope in chondrite-normalized REE patterns (tables 1-4 and 4-2).

Classification and Trends

Total alkali versus silica (TAS) Geochemical classification diagram indicates that adakitic rocks fall within the dacite, rhyodacite, and rhyolite fields, while normal calc-alkaline rocks are classified as basalt, basaltic andesite, and andesite (Le Bas et al., 1986) (Fig. 5).

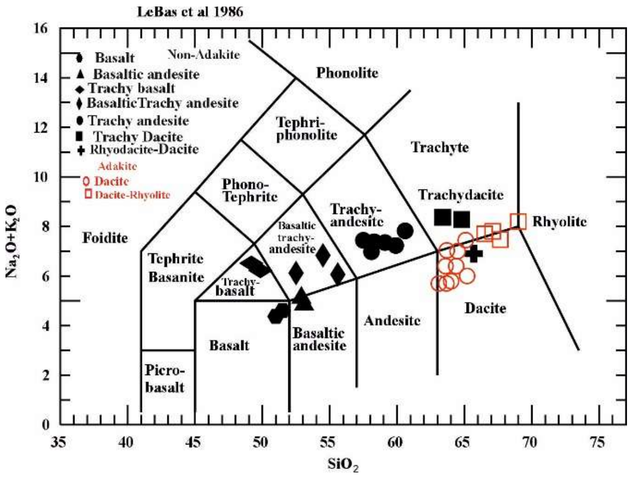

Figure 5. Plotting of samples from volcanic rocks on the discrimination diagram for different rock types (Le Bas et al., 1986).

On Harker variation diagrams, both groups show positive correlations for K_2O, Na_2O, Zr, Rb, Nb, and Th. These trends highlight the role of crystal fractionation in magma evolution (Fig. 6).

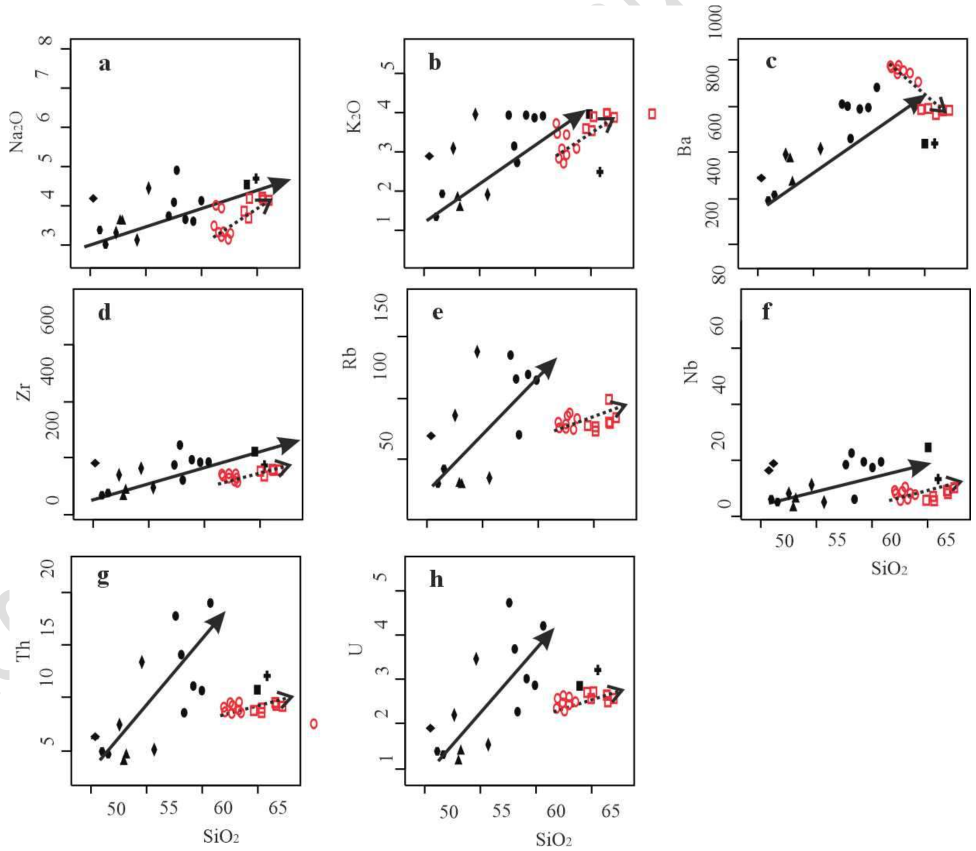

Figure 6. The harker variation diagrams of element vs. SiO_2 for the studied samples

(symbols like Figure 5)

6. Discussion

6.1. Tectonic setting

6.1.1. Tectonic setting of the adakitic rocks

The adakitic rocks in the area exhibit geochemical characteristics such as high Sr, Sr/Y, and La/Yb ratios, and low MgO, Y, and Yb values, that distinguish them from normal calc-alkaline rocks; in addition, the enrichment of LREEs and LILEs, along with the depletion of HREEs, Nb, and Ti, and the absence of a negative europium anomaly, indicate their similarity to adakitic or adakite-like rocks formed in subduction zone settings.

The Y versus Sr/Y discriminant diagram (Defant and Drummond, 1990) successfully separates adakitic rocks from normal calc-alkaline samples, with Sr/Y values higher than 32 but lower than 134, consistent with adakitic characteristics (Fig. 7a). Furthermore, the La_N/Yb_N versus Yb_N diagram (normalized to chondrite) (Martin, 1999) shows that some samples fall in the common range between normal arc and adakite signatures, suggesting that they formed in active continental margin settings (Fig. 7b).

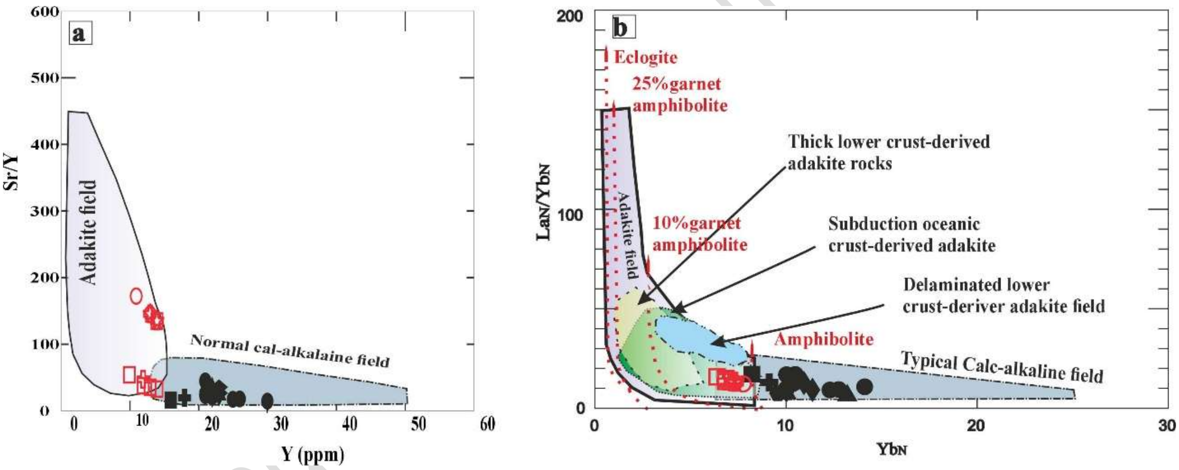

Figure 7. Position of the samples on the: a) Y vs. Sr/Y diagram (Defant and Drummond, 1990) , b) LaN/YbN vs. YbN diagram (Nakamura, 1974) for the separation of normal calc-alkaline rocks from adakites (Martin, 1999) with the melting curves of amphibolite and eclogite (Wang et al., 2002).

symbols like Figure 5.

Adakitic rocks are found in a wide range of tectonic settings in both orogenic and post-orogenic settings (Eby, 1992; Xu et al., 2002) , such as oceanic islands, continental rifts, stable continental crusts and (Xu et al., 2002; Zhang et al., 2007) On the tectonic diagrams, the adakitic samples are located in the volcanic acidic arc field (Fig. 8 a,b).

The adakitic rocks fall within the volcanic acidic arc field on tectonic discrimination diagrams (Pearce et al., 1984), further supporting their formation in subduction-related environments. The geochemical evidence suggests that the adakitic rocks are associated with subduction of oceanic lithosphere, which is consistent with other studies that have identified adakitic magmatism in a variety of tectonic settings, including oceanic islands, continental rifts, and stable continental crusts.

6.1.2. Tectonic setting of studied normal calc-alkaline rocks

The Nb-Zr-Ce/P_2O_5 and Ce/P_2O_5 vs. TiO_2 diagrams support the classification of the normal calc-alkaline rocks as continental arc derived (Fig. 8c, d). These results are consistent with the regional tectonic setting of the Alborz Belt, which was influenced by subduction and collision of the Para-Tethyan oceanic lithosphere.

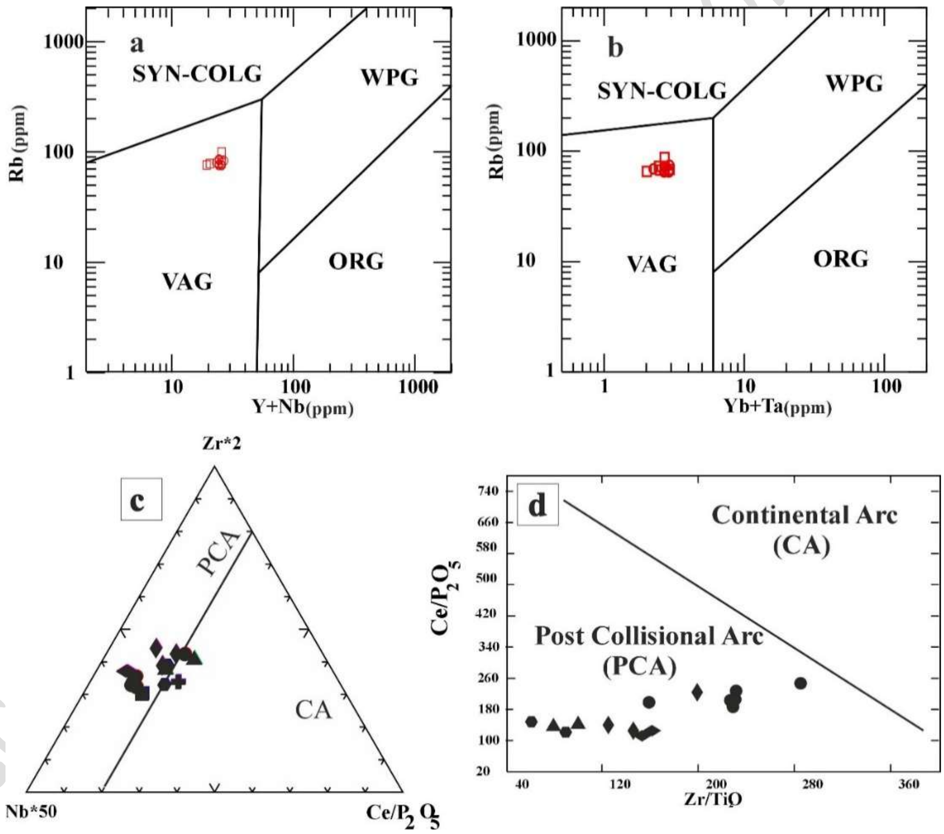

Figure 8. The adakitic samples on the: a and b) logarithmic diagrams for discrimination of the tectonic settings of granitoids (Pearce et al., 1984). SCG: orogenic granites; WPG: within plate granites; VAG: volcanic arc granites; ORG: mid-ocean ridge granites, and Non-adakitic samples on the; CA: Continental Arc; PCA: Post Collisional Arc; c) Nb-Zr-Ce/P_2O_5 (Müller et al., 1995); d) Ce/P_2O_5 vs. Zr/TiO_2 (Müller et al., 1995). symbols like Figure 5.

6.2. Petrogenesis of the rocks

6.2.1. Origin of the adakitic magmatism

Adakites are acidic to intermediate calc-alkaline rocks with a range of andesite, dacite to rhyodacite, which are formed by melting of a portion of a hot and young subducted slab (less than 20 million years old) at a depth equivalent to the pressure of the eclogite-amphibolite facies , so, adakites would typically form in arcs. Today, in addition to the melting of warm and young oceanic crust (Defant and Drummond, 1990), other sources for the production of adakitic magma have been proposed by researchers.

Therefore, to determine the exact origin of these rocks, it is necessary to study their geochemical properties. These rocks are generally divided into four groups: A) high SiO_2 adakites (HSA), B) low SiO_2 adakites (LSA), C) continental adakites, and D) Archean adakites. High SiO_2 adakites (HSA) are the result of direct melting of the subducted basaltic crust, and low SiO_2 adakites (LSA) are the result of partial melting of the metasomatized garnet mantle (due to melts released from the subducted slab).

The adakitic rocks in this study exhibit HSA characteristics, on the Martin et al., (2005) diagrams (Fig. 9 a,b,c), also, on the spider diagram normalized to N-MORB, these rocks are similar to those of high SiO_2 adakites (HAS) (Fig. 10 d). These rocks are similar to high SiO_2 adakites formed by the direct melting of basaltic oceanic crust.

High SiO_2 adakites (HSA) exhibit geochemical characteristics of, 56 <SiO_2, low Y and Yb (Yb< 1.9 and Y< 18) and relatively high Sr (Sr >300 ppm), 40 <Sr/Y and $(La/Yb)_N$ >10 (Moyen, 2009). Also, HSA, in the chondrite normalized diagrams, shows a concave pattern with a Yb/Lu ratio of about 5 (Moyen, 2009). Low SiO_2 adakites (LSA) are characterized by SiO_2 between 50 and 60 wt%, 100< Sr/Y <300, 40 <La/Yb< 80, and Yb/Lu about 10 contents (Moyen, 2009). Continental adakites are characterized by a wide range of SiO_2 (from less than 60 to more than 75 wt%), low value of Y and Yb, Sr/Y (150-150) and K_2O/Na_2O about 1 (Xiao et al., 2007). Archean adakites are found in the Greenstone belt as a result of the subduction and melting of the subducted slab. They are usually felsic and have high Na_2O low K_2O content and high Sr/Y (Moyen, 2009). The adakitic rocks with SiO_2>61 wt.%, low content of Y and Yb (Y<14 ppm and Yb< 1.6 ppm), high Sr (450 – 1883 ppm), 47< Sr/Y< 171 and 5.1< Yb/Lu<6.2 show HAS characteristics.

Several models have been proposed for the origin of adakitic magmas: 1- Crystallization and assimilation process from a basaltic melt (Macpherson et al., 2006; Guo et al., 2007), 2- Partial melting of thickened mafic crust (Atherton and Petford, 1993; Xu et al., 2002; Guo et al., 2007), 3- Partial melting of the lower continental crust due to delamination (Zhai et al., 2007; Xu et al., 2002), 4- Partial melting of the lower crust due to the penetration of hot basalts (Rapp et al., 1999; Khodami et al., 2010; Castillo, 2012).

Subducted crust-derived magmas (with subducted sediments), have a high ratios of Sr/Ce , Th/Ce >0.15 (Hawkesworth et al., 1997) and Nb/Zr >0.05 (Elburg et al., 2002). The ratios of Th/Ce, Nb/Zr and Sr/Ce in the adakitic samples are 0.16, 0.05 and 27.67, respectively, confirming the role of subducted crust in adakitic magma production. The Rb/Sr values in the samples are also low (about 0.01 to 0.04), similar to the adakites derived from melting of the subducted slab. The samples on the Th and SiO_2 vs. Th/Ce diagram are adakites with subduction origin or those of magmatic arcs (Fig. 9 d, e, f, g, h).

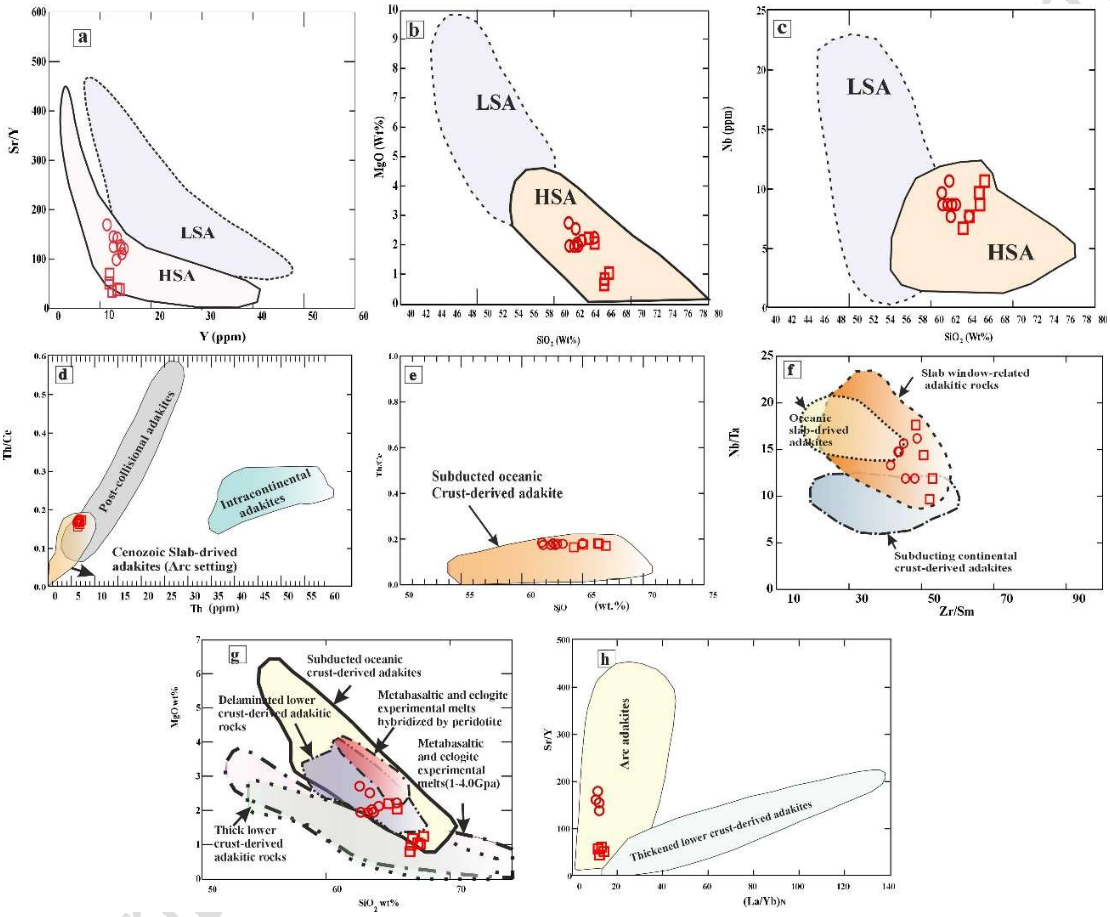

Figure 9. Distinguishing diagrams of High SiO_2 adakites (HSA) and low SiO_2 adakites (LSA) (Martin et al., 2005). All Studied adakite samples fall within the HAS field (a, b, c). d) Th vs. Th/Ce diagram (Guo et al., 2007) ; e) SiO_2 vs. Th/Ce diagram (Wang et al., 2008); f) Zr/Sm vs. Nb/Th diagram (after Defant and Drummond, 1990), the field of adakites derived from subducted continental crust and adakites derived from subducting oceanic slabs (Wang et al., 2008) and the field of adakites related to the tectonic window of (Eyuboglu et al., 2012). g) SiO_2 vs. MgO diagram and h) of Sr/Y vs. $(La/Y)_N$ diagram (the range of continental adakites and adakites of subduction zones taken (Liu et al., 2010)); Range of experimental eclogite and metabasaltic melts (Gpa1-4) (Rapp and Watson, 1995; Prouteau et al., 1999; Skjerlie and patiño douce, 2002) and range of experimental hybrid eclogite and metabasalt melts (Rapp et al., 1999). Symbols like Figure 5.

According to the proposed diagram of Defant and Drummond (1990), the adakites are produced with 5% to 10% amphibolite garnet partial melting (Fig. 7b). All samples show parallel trends of $(Ce/Yb)_N$=1.7-9.6, enrichment of LILEs, Pb, and depletion of HFSE, Ti, Nb (Fig. 14 a, b, c). Specific negative anomalies for Nb, Ti and strongly positive anomalies for Pb are observed, similar to subduction-zone related magmatism (Gill, 1981; Willson, 1989) and suggest involvement of fluids derived from subducted slabs or subducted deposits (Yan et al., 2008). No Eu anomalies are found in the samples, probably because to the fact that the magmatic evolution that formed the rocks in this area did not differentiate plagioclase (Sarem et al., 2021).

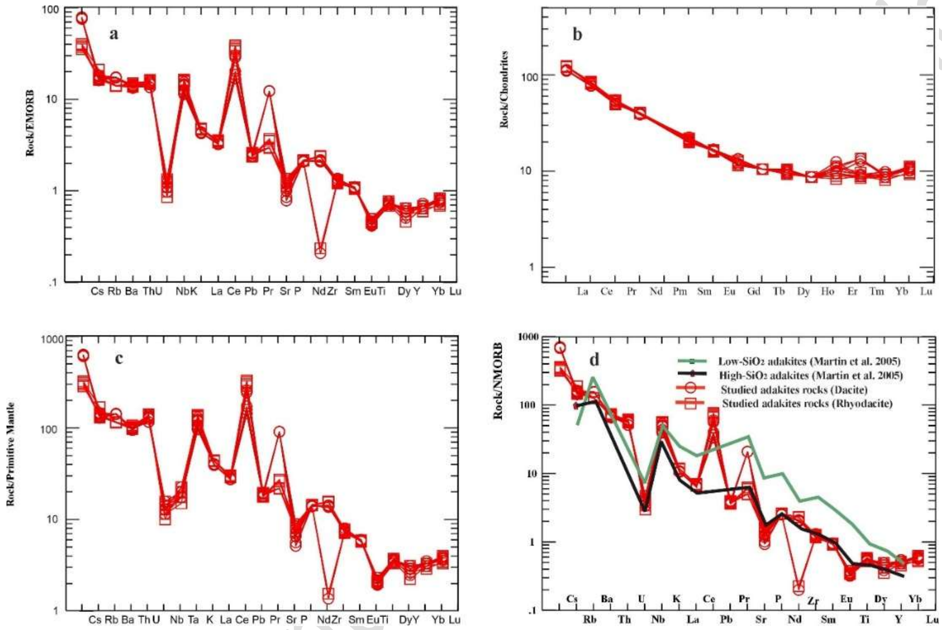

Figure 10. Normalized REE element patterns for the adakitic rocks to a) E-MORB (Sun and McDonough, 1989), b) Chondrite, c) Primitive mantle, d) N-MORB. Symbols like Figure 5.

6.2.2. Source and nature of normal calc-alkaline magma

On the chondrite-normalized REE pattern (Sun and McDonough, 1989), all rocks show linear and homogeneous sub-parallel profiles with a moderate positive slope from HREE to LREE (low field strength elements) with $(La/Yb)_N$ =4.6 – 15.4 (Fig. 11 a). In general, enrichment in the LREE relative to HREE is a characteristic feature of subduction zone-related rocks (Winter, 2001; Seghedi et al., 2004; Yang and Li, 2008), so in the volcanic rocks, the depletion of HREE is due to partial melting of metamorphosed subducted oceanic crust and remaining HREE-rich accessory minerals (i.e., garnet), such as a residual phase in the magma source. On the spider diagram normalized to the primitive mantle (Sun and McDonough, 1989), the volcanic rocks show relative enrichment of Pb, Zr, Cs, U, Th and Rb while with negative anomalies of Nb, Nd, Ta, P and Ti (Fig. 11 c), indicating the role of subducted fluids metasomatized in the source rocks (Seghedi et al., 2004; Yan et al., 2008)

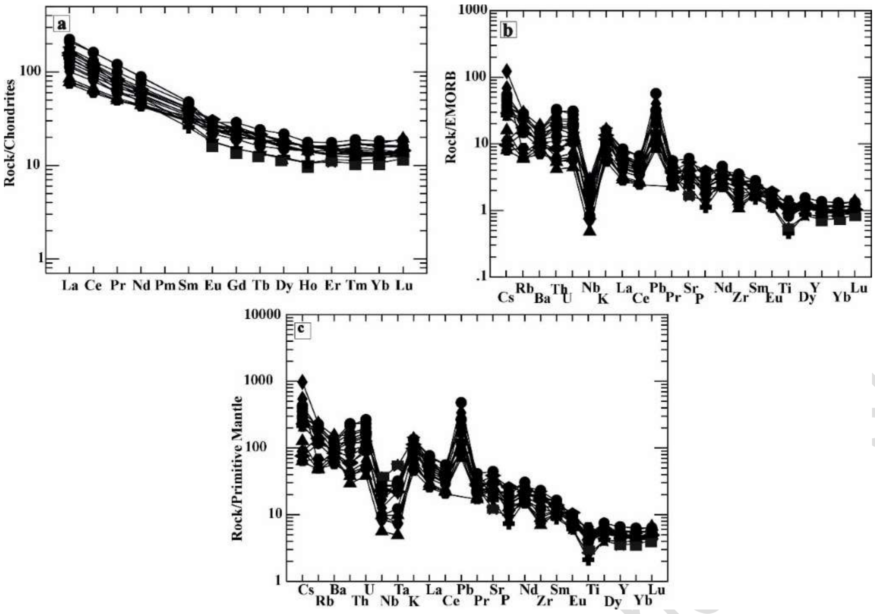

Figure 11. Spider diagram a) Chondrite-normalized REE patterns for the Rostam-Abad volcanic rocks, Normalization values are from (Sun and McDonough, 1989); b) Trace element concentrations normalized to the composition of investigated volcanic rocks relative to E-MORB; c) Primitive mantle normalized diagrams of the studied volcanics, MORB data from (Sun and McDonough, 1989). Symbols like Figure 5.

The normal calc-alkaline volcanic rocks on the chondrite normalized diagram show a very small negative anomaly of Eu, which may indicate the subduction zone dependent nature of the calc-alkaline (Martin, 1999; Yang and Li, 2008). The depletion of Nb and Ta relative to LILE is related to the addition of fluids containing this compound or the persistence of Nb and Ta in the residual phases at the source (Temizel and Arslan, 2008). The Pb positive anomaly indicates mantle wedge metasomatism with fluids released from the subducted oceanic crust or contamination of the magma with the continental crust (Kamber et al., 2002). Enrichment of U and Th in the samples has been attributed to the addition of pelagic sediments or altered oceanic crust (Fan et al., 2003).

As the degree of partial melting increases, the ratios of highly/moderately incompatible elements (such as Ba/Zr and P_2O_5) decrease (Abdel-Rahman and Nassar, 2004). On the other hand, the ratio of Zr/Y is not affected by moderate amounts of fractional crystallization (Abdel-Rahman and Nassar, 2004), Zr is more incompatible in mantle phases than Y, so, the variation of Zr/Y vs. Zr or FeO can be used to illustrate petrogenetic processes such as partial melting. The positive correlation of Zr/Y vs. Zr suggests that partial melting processes play important role in producing the range of observed magma compositions (after Pearce and Norry, 1979) (Fig. 12a). On the Ba/Y vs. Ba diagram, the linear positive trend is a function of partial melting degree, on this diagram, all normal calc-alkaline samples show a linear positive trend (Fig. 12 b) (Abdel-Rahman and Nassar, 2004), the observed relative fractionation in such a ratio is a function of the degree of partial melting degree. Relative fractionation of HFSE is a common feature in both continental and oceanic basalts (Moghazi, 2003), and is thought to be a function of the amount of residual garnet and clinopyroxene in the mantle source as a result of different degrees of partial melting (Moghazi, 2003). Since Y is retained in garnet, the negative correlation such as Ce/Y and Nb/Y ratios (Moghazi, 2003) vs. Zr/Nb in the rocks (Fig. 12 c, d) suggests that partial melting may explain the variation in this.

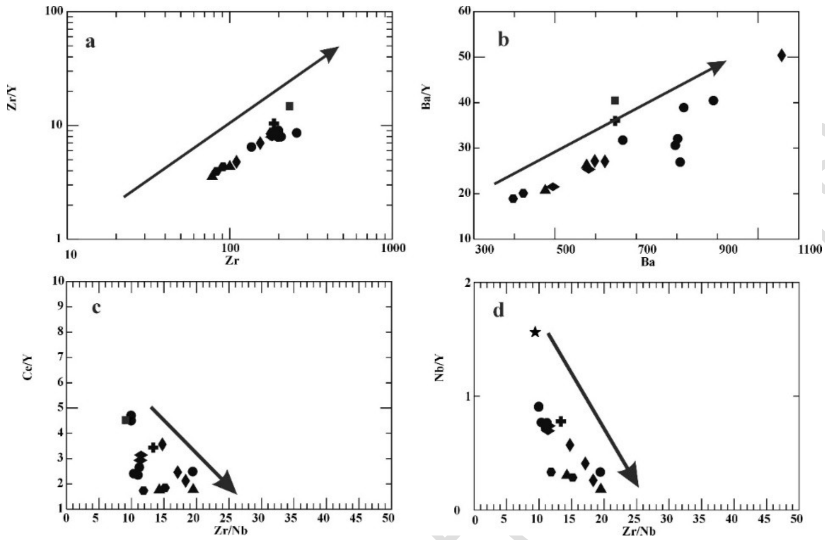

Figure 12. Variation diagrams between a) Zr vs. Zr/Y (after (Pearce and Norry, 1979)); b) Ba vs. Ba/Y (Abdel-Fattah et al. 2003); c) Zr/Nb vs. Ce/Y and Nb/Y (Moghazi, 2003). Symbols like Figure 5.

In addition, the following geochemical evidence in the samples indicates the role of the fractional crystallization process in their magma formation: 1) increasing linear trends of Na_2O, K_2O, Rb, Nb, Zr, Th, and U and decreasing linear trends of Al_2O_3, MgO, CaO, TiO_2, Sr, V and Co with increasing SiO_2 (Fig. 6), 2) linear trend between Rb such as incompatible element versus incompatible elements (Y and Nb) (Fig. 13 a, b), 3) parallel trend of the REE normalized patterns, 4) with increasing of magmatic fractional crystallization and decreasing of MgO, the ratio of CaO/Al_2O_3 decreased. Since the ratio of CaO/Al_2O_3 in clinopyroxene is 10 times that of plagioclase, the ratio of CaO/Al_2O_3 decreases with the fractionation of clinopyroxene (Le Roux et al., 2002), on the other hand, olivine fractionation, cannot change of the CaO/Al_2O_3 ratio, so this ratio only by taking the Mg in the olivine, MgO content in the remaining melt decreases. This shows the role of olivine and clinopyroxene fractionation in the evolution of the rocks (Fig. 13 c), 5) Al_2O_3/CaO variations vs. SiO_2 shows that fractionation of clinopyroxene more than plagioclase is an important factor for the evolution of magma (Zhu et al., 2007), (Fig. 13 d), 6) Increasing the Ba/Rb and Ba/Sr ratios with increasing SiO_2 between different rock series (Gill, 1981) (Fig. 13 e, f) and the direct linear relationship of the incompatible elements (Nb, La, Zr) with La/Sm ratio can be considered as a reason for the crystal fractionation of magma, (Fig. 13 g, h, i).

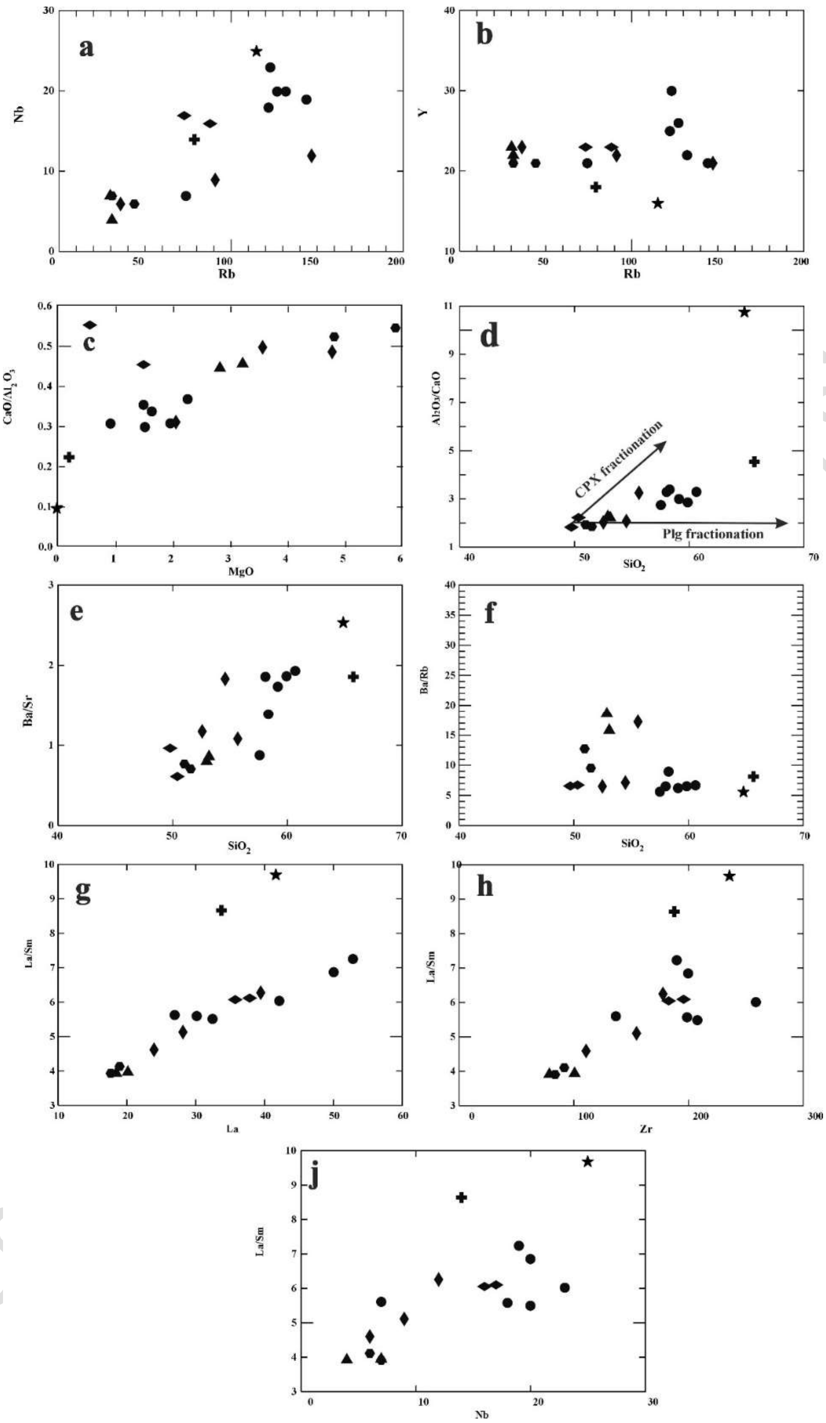

Figure 13. Two variation diagrams for the Rostam-abad non-adakitic rocks, a, b) Nb and Y vs. Rb; c) Al_2O_3/CaO vs. MgO; d)CaO/Al_2O_3 vs. SiO_2 (DiCheng et al., 2007); e, f) Ba/Rb and Ba/Sr ratios vs. SiO_2 (Gill, 1981); g, h, i) Incompatible elements (Nb, La, Zr) vs. La/Sm (Moghazi, 2003). Symbols like Figure 5.

Also, in the Ashwal et al. (2016) diagram which is drawn based on the studies on the experimental melt, the normal calc-alkaline samples show a similar trend of the crystallization of the experimental basaltic melt from the basic to the felsic samples. Therefore, it seems that all the normal calc-alkaline samples are the result of the crystal fractionation process from the same basaltic melt. Thus, first the basaltic components and then the intermediate and finally, in the upper layers, more felsic and acidic components are formed (Fig. 14).

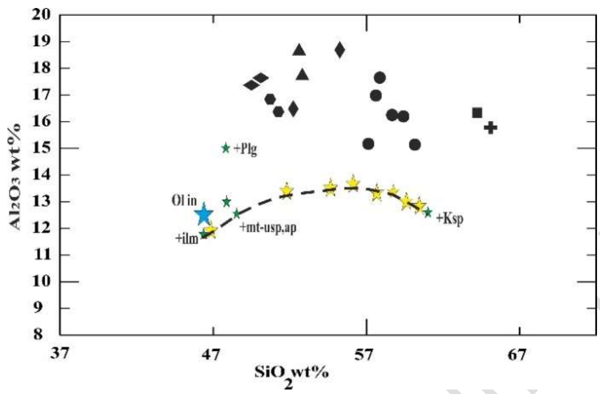

Figure 14. Harker variation diagrams showing the results of fractional crystallization modelling of an assumed basaltic parental liquid (blue star), using PELE software (Boudreau, 1999). Successive residual liquid compositions are shown by yellow stars at intervals of 20 °C. The appearance of liquidus mineral phases is shown by green stars (ol: olivine; plag: plagioclase; cpx: clinopyroxene; ilm: ilmenite; mt-usp: magnetite; ap: apatite; Ksp: K-feldspar). Starting conditions are as follows: T= 1305.6 °C, P =1 kbar, H_2O =0.21 wt %. The fractionation model succeeds in the non-adakitic rocks. Symbols like Figure 5.

Samples with the highest Ce/Y and Nb/Y and the lowest Zr/Nb show a lower degree of partial melting. On the La vs. La/Sm and the La/Yb vs. La diagrams (Fig. 15a, b) (Wang et al., 2007), all the normal calc-alkaline samples show a trend between partial melting and crystal fractionation. Thus, it appears that both processes (partial melting and crystal fractionation) play an important role in controlling the compositional diversity and formation of the parent magmas of these rocks, but partial melting is more important than crystal fractionation.

Crustal contamination is a secondary process that may have contributed to the chemical composition of the rocks. Some chemical parameters can be used to assess the degree of contamination. LILE (such as Rb, Cs, K, and K) are incompatible elements and do not enter to the structure of minerals such as plagioclase, pyroxene, and opaque minerals, therefore, any increase and any change in the amounts of these elements in the rocks, is due to crustal contamination in the magma that forms the rocks. Crustal contamination can also increase the Th/Yb ratio relative to that of Ta/Yb because of a higher abundance of Th relative to Ta in the crustal rocks (Aldanmaz et al., 2000) (Fig. 15c). Crustal contamination affects Th more than Ta and Yb so the samples with crustal contamination have high Th/Yb values (Moghazi, 2003). Yb is used as a normalization factor to minimize the effects of fractional crystallization and crystal accumulation (Pearce, 2005;

Aldanmaz et al., 2008). The linear trend of the samples is also consistent with the enrichment trend of subduction lava zones. On the Ba/Th versus Th/Nb diagram, the studied normal calc-alkaline samples show low Ba/Th values and approximately different values of Th/Nb (Fig. 15d). The high of Th/Nb values indicate the widespread involvement of high crustal materials in the formation of these rocks. In other words, these ratios indicate the intensity of subducted products or crustal materials in the magma (Pearce, 2005). The vertical trend of the normal calc-alkaline samples examined shows the characteristic of enrichment by subducted fluids or crustal contamination on the Temel et al. (1998) plot (Fig. 15e).

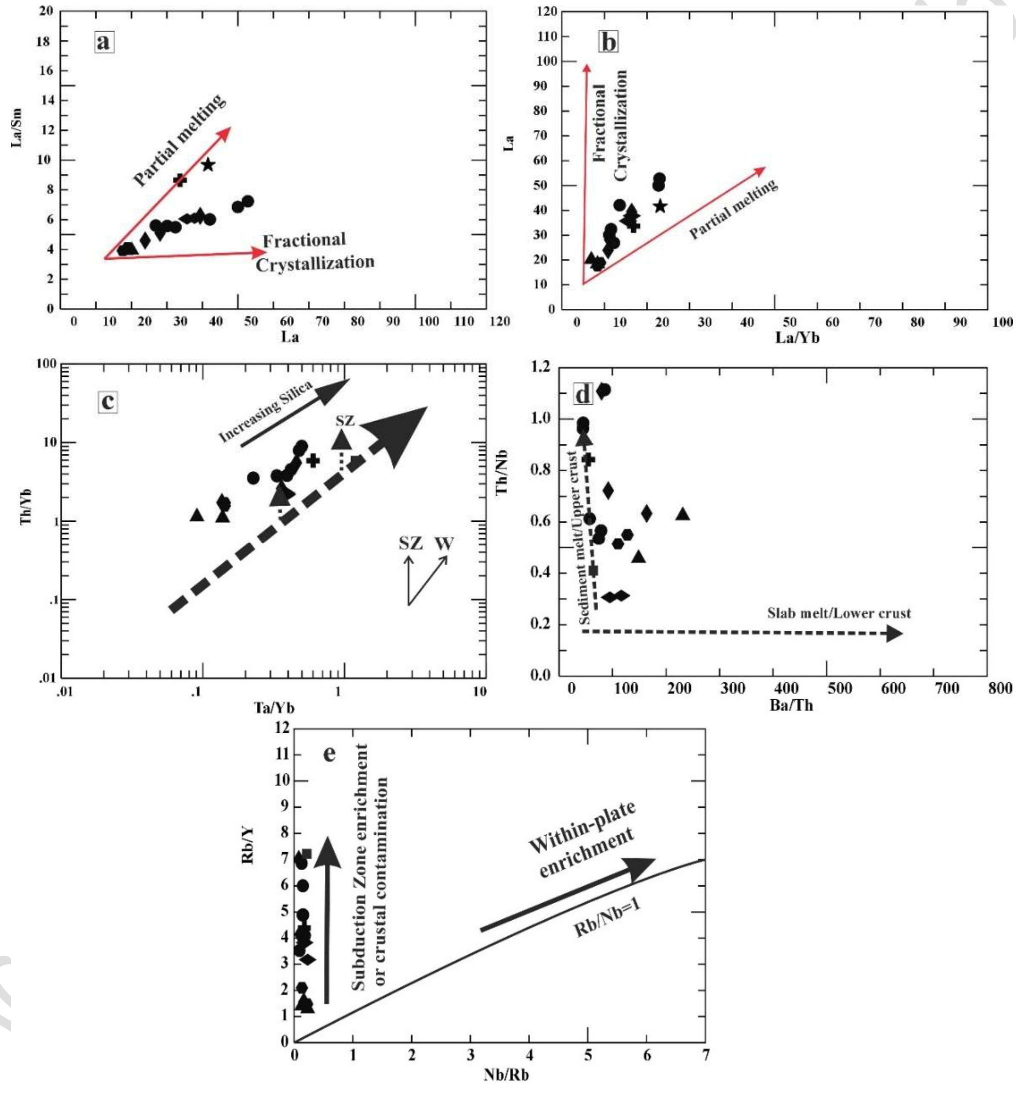

Figure 15. a,b) Diagrams of La vs. La/Sm and the La/Yb vs. La (Wang et al., 2007), all the non-adakite rocks show a trend between partial melting and fractional crystallization; c) Th/Yb vs. Th/Yb (Pearce, 1983); d) Ba/Th vs. Th/Nb (Orozco-Esquivel et al., 2007); e) Nb/Rb vs. Rb/Y (Temel et al., 1998). The diagrams indicate the subduction zone enrichment trend for these rocks. Symbols like Figure 5.

The crustally contaminated rocks have a K/P ratio>7, La/Ta>22, and La/Nb> 1.5 (Abel-Fattah et al. 2004), so the low values of such elemental ratios in the studied rocks (K/P=9.7-37.65; La/Ta=18.9-79.66; La/Nb=1.66-3.98) suggest that the crustal contamination played an important role of during magma evolution (Abel-Fattah et al., 2004).

Fig. 16a shows that the La concentrations and La/Sm ratios of the rocks are greater than those that could be produced by direct melting of the DMM (Depleted MORB Mantle), even when the degree of partial melting is very small (0.1%). Extrapolation of the best-fit partial melting trajectories drawn for the studied rocks gives degrees of partial melting between 1 and 10% of a mantle source (on the mantle array) with La concentration and La/Sm ratio significantly higher than both DMM and PM (Primitive Mantle). Therefore, it appears that a mantle source enriched in LREE to DMM composition is required to produce the magma of this rock, and therefore a one-step melting of DMM (or PM) cannot produce this magma. The Sm/Yb ratio vs. Sm can be used to constrain the source mineralogy of the alkaline magmas because Yb is compatible with garnet but not with clinopyroxene. This diagram shows that the rocks are shifted from the spinel-garnet-lherzolite melting trend (mantle array) to higher Sm/Yb ratios than spinel-lherzolite melting trajectories and plot between garnet- and garnet+spinel-lherzolite (Fig. 16b) that indicates the presence of a garnet residue in their source region. Fig. 16c shows Sm/Yb vs. La/Sm and variable degree of partial melting of garnet-lherzolite and spinel-lherzolite sources, also shows reference compositions representing possible asthenospheric mantle sources (N-MORB and PM, (Sun and McDonough, 1989)), and distinguishes near to garnet-spinel-lherzolite sources are shown on that. Partial melting of the spinel-lherzolite mantle source produced a melt with similar Sm/Yb ratios to the mantle and does not change the Sm/Yb ratio because both Sm and Yb have similar partition coefficients, whereas with increasing degrees of partial melting, the La/Sm ratios and Sm contents of the melts may decrease (Seghedi et al., 2004). In contrast, a small (or moderate) degree of partial melting of a garnet-lherzolite source (with garnet residues) produces melt with significantly higher Sm/Yb ratios than the mantle source. Based on this diagram, studied normal calc-alkaline rocks are plotted in the spinel+garnet–lherzolite trend with 1-15% partial melting (with slightly higher Sm/Yb ratios). These diagrams show that the source of the rocks is enriched in LREE relative to DMM (and PM). The simplest model to explain the REE systematics of the rocks thus involves garnet+spinel mantle mineralogy (but mostly garnet rather than the spinel). The most diagnostic feature of residual garnet is the heavy rare earth element (HREE) fractionation due to their strong partitioning into garnet (Abdel-Rahman and Nassar, 2004). This suggests a final melt segregation depth of about 80 km (Moghazi, 2003). The normal calc-alkaline samples in the Ce/Yb versus Ce diagram show, that the depth of partial melting of the source magma of these rocks is estimated to be 110 to 110 km (Fig. 16 d). Thus, the samples appear to be derived from 1-15% partial melting of garnet-spinel-lherzolite magma at a depth of >100 km.

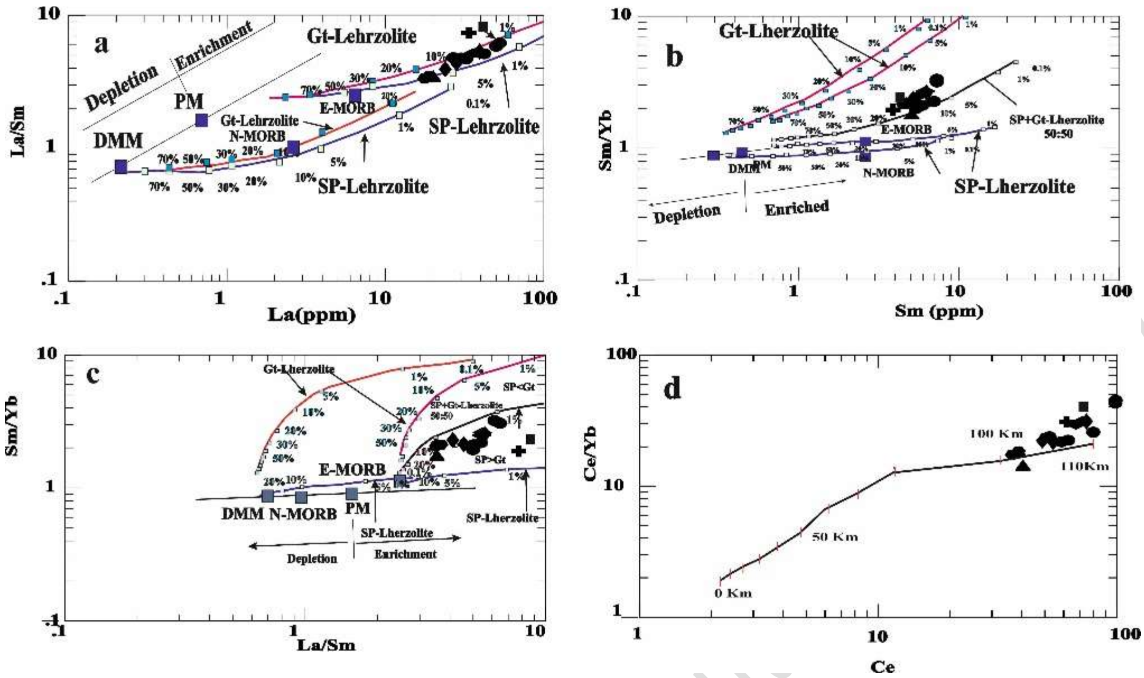

Figure 16. a) La/ Sm vs. La diagram. linear array showing a linear mixing between enriched (EM) and depleted (DM) melts (Aldanmaz et al., 2000) ., b, c) Sm/ Yb vs. Sm and Sm/Yb vs. La/Sm diagrams showing melting curves obtained using the non-modal batch melting equation of (Shaw, 1970) and the method proposed by Albarede (1995). Melt curves are drawn for spinel lherzolite and garnet lherzolite with melt mode of Ol 0.53+Opx0.27+Cpx0.17+Sp0.03 and Ol0.60+Opx0.20+Cpx0.10+Gt0.10. Mineral–matrix partition coefficients are from (McKenzie and O'nions, 1991) d) Position of normal calc-alkaline studied rocks on the Ce vs. Ce/Yb logarithmic diagram (Ellam and Cox, 1991) (Symbols are the same as in Figure 5).

6.3. Geodynamic implications

The study area, located in the Alborz Mountains of northern Iran, is part of the Alborz Orogeny, a region of active deformation, that is one of the best examples of an active continental margin in Iran. Based on previous studies, the Cenozoic magmatism of the Alborz orogenic belt is generally considered to be related to a post-collision setting following northward subduction and closure of the Neotethys oceanic lithosphere between Eurasia and the Central Iranian Plate during the Paleocene (Asiabanha et al., 2009; Ghasemi et al., 2012; Bahajroy and Taki, 2014; Teimouri et al., 2018; Akmali et al., 2019). However, the recent geological and geochemical studies on the Late Mesozoic-Cenozoic magmatic rocks in the Alborz orogenic belt do not support this idea to explain the origin of the source of magmatism (Kaz'min and Tikhonova, 2006; Salavati et al., 2009; Hakimi Asiabar, 2010). In the present study, we propose a tectonomagmatic model to explain the origin of Late Cenozoic magmatism and recent tectonic activity in the area.

The present study in the Alborz arc in the province of Guilan has revealed two different types of adakitic and normal arc magmatism. Delamination or partial melting of the thickened lower crust after the collision in the south cannot explain the change of Tertiary adakitic and non-adakitic magmatism in the north. In addition, geochemical evidence from adakitic samples indicates negative P, Sr, Ba and Eu anomalies. According to some researchers (Pe-Piper et al., 2002), this may indicate that the lower crust did not play a role in the formation of its magma. This suggests that the complex was formed by partial melting of magma as a result of oceanic crustal subduction and therefore the studied adakites are not of mantle origin (LSA adakite) and continental origin (continental adakite).

A subduction zone associated with the closure of the Para-Tethyan Ocean with a North dip in the Cenozoic has also been reported in the south of the area and in the southern basin of the Caspian Sea in previous studies (Kaz'min and Tikhonova., 2006; Salavati et al., 2009; Hakimi Asiabar, 2010). These studies indicate that the collision of the Eurasian and Central Iranian plates began in the Early Cenozoic. This collision can also be seen in the southern Black Sea in Turkey and in the Caucasus (Pontides - Lesser Caucasus - Albroz Magmatic Arc) (Eyuboglu et al., 2012) (Fig. 17a).

Eyuboglu (2018) believes that the entire northern margin of the East Pontic-Lesser Caucasus-Albroz magmatic arc is an active continental margin zone during the Cenozoic, created by the southward subduction of the Paratethys oceanic lithosphere, and as a result of this process the Caspian Sea basin separated from the Black Sea basin. Continued continental-arc collision caused crustal thickening and partial melting of the mafic part of the thickened crust. This led to the formation of younger adakitic rocks. Continued subduction led to slab break-up and the opening of an asthenosphere window beneath a magmatic arc.

Thorkelson and Breitsprecher (2005) proposed that both adakite and normal arc rocks are produced near the trench when a spreading mid-ocean ridge subducts (slab window setting). They proposed that typical arc mafics may form along the plate margins between 5 and 65 km deep, whereas adakites form near the plate margins between 25 and 90 km deep in the slab window setting.

All this evidence supports the “Ridge-Trench” tectonic model to describe the tectonomagmatism in the study area. According to this model, as a result of the subduction of the mid-ocean ridge and the opening of the tectonic window, OIB magmatism formed with A-type granitoids in the center, and at the arc margin and near the tectonic window, adakitic rocks formed from melting of the subducted crust (Zhang, 2014).

In addition to the studied adakitic and normal arc rocks, A-type granitic bodies and basalt-andesitic volcanic rocks of the subduction-related magmatic complex and Neogene alkaline rocks have been reported in the north of this region (Taki et al., 2009; Rezania ye Komachaly et al., 2022; Salavati et al., 2012; Salavati et al., 2013).

All this evidence confirms the possibility of a "ridge-trench" tectonic model in the study area and the existence of a subduction zone during the Eocene in the southern Caspian Sea basin.

All the information suggested that the Late Paleocene–Early Eocene adakitic rocks were generated, by slab window processes, during ridge subduction in a subduction zone. Therefore, we considered the geodynamic models proposed by Eyuboglu et al., (2012) for the origin of Late Paleocene–Early Eocene adakitic rocks in the Pontides orogenic belt, as well as for the generation of the Neoproterozoic–Paleozoic orogenic belt of Central Asia. In addition, the existence of a south-dipping reverse fault system along the entire southern coast of the Caspian Sea supports a southward subduction model for the origin of the Alborz orogenic belt and also slab window process for the origin of the late Paleocene–early Eocene adakitic and calc-alkaline normal arc activity (Hakimi Asiabar, 2010). Thus, there is evidence that a collision between Eurasia and the Central Iranian Plate was initiated in the Early Cenozoic. This collision is also observed in the southern part of the Black Sea in Turkey and the Caucasus (Pontides-Lesser Caucasus-Albroz magmatic arc) (Eyuboglu et al., 2012) (Fig. 17a).As a result of this process, the Caspian Sea basin was separated from the Black Sea basin. Continued continent-arc collision caused crustal thickening, and partial melting of the mafic lower part of a thickened crust produced the younger adakitic rocks. As subduction continued, slab rupture occurred and an asthenospheric window was opened beneath a magmatic arc. Thorkelson and Breitsprecher (2005) suggested that when a mid-ocean spreading ridge subducts (slab window setting), both adakite and normal arc rocks are produced near the trench. Thorkelson and Breitsprecher (2005) suggested that normal arc melts may form along the plate margins at depths of 5-65 km, whereas adakite melts form near the plate margins at depths of 25-90 km in a slab window setting. In the study area, partial melting of the subduction-modified mantle wedge and development of alkaline magmatic rocks are exposed in the northern part of the Gilan in Albruz magmatic arc (Fig. 17b) (Rezania ye Komachaly et al., 2022). In addition, slab break-up of the subducted Tethyan oceanic lithosphere would have led to uplift of the region on the reverse fault extending along the northern margin of the magmatic arc.

7. Summary and Conclusions

Based on all field studies, petrographic and geochemical data of the Paleogene volcanic rocks have been obtained:

The field studies confirm the presence of Paleogene volcanic and sub-volcanic rocks, ranging from dacite to trachydacite, rhyodacite, and rarely rhyolite, in the southern Caspian Sea area and southern Gilan province, south of Rostamabad and north of Rudbar.

The geochemical characteristics show that the studied rocks can be divided into two main groups: The first group is similar to adakitic and adakitic-like rocks with higher values of Sr, Sr/Y and La/Yb and lower values of MgO, Y and Yb, with enrichment of LREE and LILE elements and depletion of HREE, Nb, Ti and absence of Eu negative anomaly, and the second group with characteristics similar to normal calc-alkaline volcanic rocks. The adakitic group is similar to the

HSA. Both adakitic and normal calc-alkaline samples were formed in the active continental margin environment.

Both processes (partial melting and crystal differentiation) played an important role in controlling the evolution of the normal calc-alkaline magmas studied. Normal calc-alkaline magmas were formed from the 1-15% melting of garnet-spinel-lherzolite magmas at depth. Based on all the field, petrographic and geochemical data, the "Ridge-Trench" tectonomagmatic model has been proposed for the formation of these rocks. According to this model, partial melting of a subducting slab associated with the southward subduction of the Para-Tethys oceanic crust (and subduction of the mid-oceanic ridge) beneath the northern margin of the Alborz Mountains has led to the formation of a mantle window beneath the continental crust. As a result, asthenospheric magmas rise through this window. Partial melting of the subducted slab at different depths and degrees, coinciding with the formation of the tectonic window in the subduction zone, has produced adakitic magmas. Meanwhile, normal arc rocks coexist in areas further away.

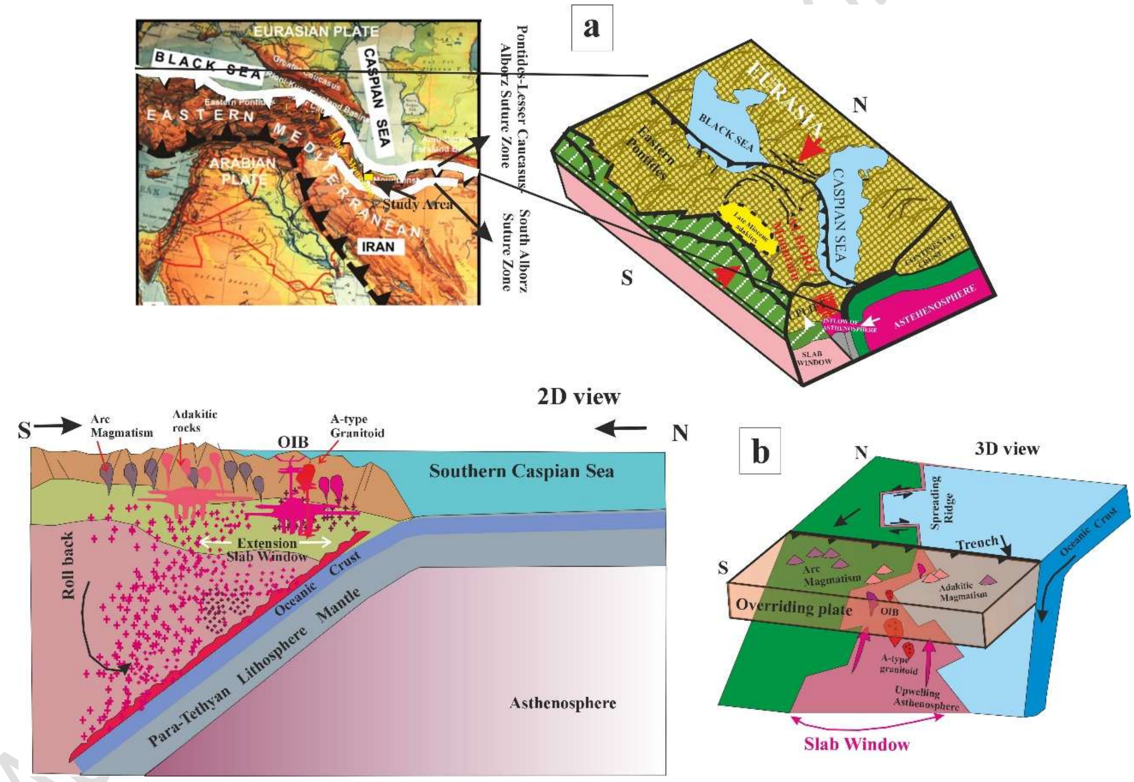

Figure 17. a) A geodynamic model for the late Cenozoic in the South Black Sea and South Caspian Sea region (modified after (Eyuboglu et al., 2012)). b) Fig 23. Proposed schematic image of the tectonomagmatic conditions for the formation of adakitic rocks in the studied area (based on the model proposed by Eyuboglu et al., (2018)).

Acknowledgments

The present study is the result of a study entitled "Petrology and geochemistry of igneous rocks in the Rostamabad-Roodbar area in the Guilan province, Northern Iran" and the authors wish to thank the Office of Graduate Studies of the Islamic Azad University, Lahijan Branch.

Author Statement

All authors contributed to the study's concept and design. Fieldwork and petrographic studies manuscript organization, and writing were carried out by Mojgan Salavati, and data interpretation was done by all the authors.

References

Abdel-Rahman A. F. M., Nassar P. E. (2004) Cenozoic volcanism in the Middle East: petrogenesis of alkali basalts from northern Lebanon. *Geological magazine* 141: 545-563. DOI: https://doi.org/10.1017/s0016756804009604

Abdolahadi A., Sheikhzakariaee S.J., Yazdi A., Mousavi S.Z. (2025) Plio-Quaternary Adakite Genesis and Post-collisional Processes: Whole Rock Constraints and Sr, Nd Isotopic Compositions in Alborz Magmatic Belt, Ardabil, Iran, *Journal of Mining and Environment*, 16(2):737-765. DOI: https://doi.org/10.22044/jme.2024.14781.2801

Akmali S., Asiabanha A., Haghnazar S. (2019) Cretaceous magmatic evolution in the Deylaman igneous complex, Alborz zone, Iran: change from extensional to compressional regime. *Geological Quarterly* 63: 757-770. DOI: https://doi.org/10.7306/gq.1500

Albarede F. (1995) Introduction to Geochemical Modeling. *Cambridge University Press* DOI: https://doi.org/10.1017/CBO9780511622960

Aldanmaz E., Pearce J. A., Thirlwall M., Mitchell J. (2000) Petrogenetic evolution of late Cenozoic, post-collision volcanism in western Anatolia, Turkey. *Journal of volcanology and geothermal research* 102: 67-95. DOI: https://doi.org/10.1016/S0377-0273(00)00182-7

Aldanmaz E., Yaliniz M., Guectekin A., Göncüoğlu M. C. (2008) Geochemical characteristics of mafic lavas from the Neotethyan ophiolites in western Turkey: implications for heterogeneous source contribution during variable stages of ocean crust generation. *Geological magazine* 145: 37-54. DOI: https://doi.org/10.1017/S0016756807003986

Ashwal L., Torsvik T., Horvath P., Harris C., Webb S., Werner S., Corfu F. (2016) A Mantle-derived Origin for Mauritian Trachytes. *Journal of Petrology* 57: 1645–1675. DOI: https://doi.org/10.1093/petrology/egw052

Asiabanha A., Bardintzeff J. (2014) Globule-rich lavas in the Razjerd district, Qazvin, Iran: a unique volcanic DOI: https://doi.org/ 10.1127/0077-7757/2009/0144fabric. *Arabian Journal of Geosciences* 7: 1907-1925. DOI: https://doi.org/10.1007/s12517-013-0842-4

Asiabanha A., Bardintzeff J., Kananian A., Rahimi G. (2012) Post-Eocene volcanics of the Abazar district, Qazvin, Iran: Mineralogical and geochemical evidence for a complex magmatic evolution. *Journal of Asian Earth Sciences* 45: 79-94. DOI: https://doi.org/10.1016/j.jseaes.2011.09.020

Asiabanha A., Ghasemi H., Meshkin M. (2009) Paleogene continental-arc type volcanism in North Qazvin, North Iran: facies analysis and geochemistry. *Neues Jahrbuch fur Mineralogie-Abhandlungen* 186: 201.

Atherton M. P., Petford N. (1993) Generation of sodium-rich magmas from newly underplated basaltic crust. *Nature* 362: 144-146. DOI: https://doi.org/ 10.1038/362144a0

Axen G. J., Lam P. S., Grove M., Stockli D. F., Hassanza-deh J. (2001) Exhumation of the west-central Alborz Moun-tains, Iran, Caspian subsidence, and collision-related tectonics. *Geology* 29: 559–562. DOI: https://doi.org/ 10.1130/0091-7613(2001)029<0559:EOTWCA>2.0.CO;2

Bahajroy M., Taki S. (2014) Study of the mineralization potential of the intrusives around Valis (Tarom-Iran). *Earth Sciences Research Journal* 18: 123-129. DOI: https://doi.org/ 10.15446/esrj.v18n2.44799

Berberian F., Muir I. D., Pankhurst R. J. and Berberian M. (1982) Late Cretaceous and early Miocene Andean type plutonic activity in northern Makran and central Iran. *Journal of the Geological Society* 139: 605–614. DOI: https://doi.org/10.1144/gsjgs.139.5.0605

Berberian M., King G. (1981) Towards a paleogeography and tectonic evolution of Iran. *Canadian journal of earth sciences* 18: 210-265. DOI: https://doi.org/10.1139/e81-019

Boudreau A. (1999) PELE—a version of the MELTS software program for the PC platform. *Computers & Geosciences* 25: 201-203. DOI: https://doi.org/10.1016/S0098-3004(98)00117-4

Castillo P. R. (2012) Adakite petrogenesis. *Lithos* 134: 304-316. DOI: https://doi.org/10.1016/j.lithos.2011.09.013

Dabiri R., Akbari-Mogaddam M., Ghaffari M. (2018) Geochemical evolution and petrogenesis of the eocene Kashmar granitoid rocks, NE Iran: implications for fractional crystallization and crustal contamination processes, *Iranian Journal of Earth Sciences* 10 (1): 68-77.

Defant M. J., Drummond M. S. (1990) Derivation of some modern arc magmas by melting of young subducted lithosphere. *Nature* 347: 662-665. DOI: https://doi.org/10.1038/347662a0

Dicheng Z., Guitang P., Xuanxue M., Zhongli L., Xinshenng J., Liquan W., Zhidan Z. (2007) Petrogenesis of Volcanic rocks in the Sangxiu Formation, Central Segment of Tethyan Himalaya:

A Probable example of Plume-Litospher interaction. *Journal of Asian Earth Sciences* 29: 320-335. DOI: https://doi.org/10.1016/j.jseaes.2005.12.004

Dokuz A., Uysal I., Siebel W., Turan M., Duncan R., Akçay M. (2013) Post-collisional adakitic volcanism in the eastern part of the Sakarya Zone, Turkey: evidence for slab and crustal melting. *Contributions to Mineralogy and Petrology* 166: 1443-1468. DOI: https://doi.org/10.1007/s00410-013-0936-8

Eby G. N. (1992) Chemical subdivision of the A-type granitoids, petrogenetic and tectonic implications. *Geology* 20: 641–644. DOI: https://doi.org/10.1130/0091-7613(1992)020<0641:CSOTAT>2.3.CO;2

Eftekhar Nejad J. (1980) Tectonic classification of Iran in relation to depositional basins. *Journal of Iranian Petroleum Society* 82: 19-28.

Elburg M. A., Van Bergen M., Hoogewerff J., Foden J., Vroon P., Zulkarnain I., Nasution A. (2002) Geochemical trends across an arc-continent collision zone: magma sources and slab-wedge transfer processes below the Pantar Strait volcanoes, Indonesia. *Geochimica et Cosmochimica Acta* 66(15): 2771-2789. DOI: https://doi.org/10.1016/S0016-7037(02)00868-2

Ellam R., Cox K. (1991) An interpretation of Karoo picrite basalts in terms of interaction between asthenospheric magmas and the mantle lithosphere. *Earth and Planetary Science Letters* 105: 330-342. DOI: https://doi.org/10.1016/0012-821X(91)90141-4

Elmi R., Arian M. A., Ashja Ardalan A., Yazdi A. (2025) Petrology of volcanism in the Alasht-Haraz road of the Alborz mountain range, south of Amol (north of Iran), *Iranian Journal of Earth Sciences*, 17(3): 1-16. DOI: https://doi.org/10.57647/j.ijes.2025.16800

Eyuboglu Y., Dudas F. O., Santosh M., Eroğlu-Gümrük T., Akbulut K., Yi K., Chatterjee N. (2018) The final pulse of the Early Cenozoic adakitic activity in the Eastern Pontides Orogenic Belt (NE Turkey): An integrated study on the nature of transition from adakitic to non-adakitic magmatism in a slab window setting. *Journal of Asian Earth Sciences* 157: 141-165. DOI: https://doi.org/10.1016/j.jseaes.2017.07.004

Eyuboglu Y., Santosh M., Yi K., Bektaş O., Kwon S. (2012) Discovery of Miocene adakitic dacite from the Eastern Pontides Belt (NE Turkey) and a revised geodynamic model for the late Cenozoic evolution of the Eastern Mediterranean region. *Lithos* 146: 218-232. DOI: https://doi.org/10.1016/j.lithos.2012.04.034

Fan W. M., Guo F., Wang Y. J., Lin G. (2003) Late Mesozoic calc-alkaline volcanism of post-orogenic extension in the northern Da Hinggan Mountains, northeastern China. *Journal of volcanology and geothermal research* 121: 115-135. DOI: https://doi.org/10.1016/S0377-0273(02)00415-8

Ghasemi A., Talbot C. J. (2005) A new tectonic scenario for the Sanandaj-Sirjan Zone (Iran). *Journal of Asian Earth Sciences* 26: 683-693. DOI: https://doi.org/10.1016/j.jseaes.2005.01.003

Ghasempour M. R., Mehdipour Ghazi J., Biabangard H., Dabiri R. (2014) Petrogenetic Evolution of Plio-Quaternary Mafic Lavas in Nehbandan (East Iran), *Iranian Journal of Earth Sciences* 6 (2): 133-141.

Gill J. B. (1981) Orogenic Andesites and Plate Tectonics. Minerals and Rocks, 390.

Golonka J. (2004) Plate tectonic evolution of the southern margin of Eurasia in the Mesozoic and Cenozoic. *Tectonophysics* 381: 235-273. DOI: https://doi.org/10.1016/j.tecto.2002.06.004

Guo Z., Wilson M., Liu J. (2007) Post-collisional adakites in south Tibet: products of partial melting of subduction-modified lower crust. *Lithos* 96: 205-224. DOI: https://doi.org/10.1016/j.lithos.2006.09.011

Hakimi Asiabar S. (2010) Collisional Tectonics of western Alborz range On the basis of Structural deformations of Dorfak-Somamous area. Ph.D. in Geology-Tectonics, *Shahid Beheshti University*, Tehran, Iran.

Hawkesworth C., Turner S., McDermott F., Peate D., Van Calsteren P. (1997) U-Th isotopes in arc magmas: Implications for element transfer from the subducted crust. *Science* 276: 551-555. DOI: https://doi.org/ 10.1126/science.276.5312.551

He X., Tan S., Liu Z., Bai Z., Wang X., Wang Y., Zhong H. (2020) Petrogenesis of the Early Cretaceous Aolunhua adakitic monzogranite porphyries, Southern Great Xing'an Range, NE China: implication for geodynamic setting of Mo mineralization. *Minerals* 10: 332. DOI: https://doi.org/10.3390/min10040332

Jung D., Küsten M., Tarkian M. (1976) Post-Mesozoic volcanism in Iran and its relation to the subduction of the Afro- Arabian under the Eurasian plate. In: Pilger, A. and Rosler, A. (eds.): Afar Between Continental and Oceanic Rifting. E. Schweizerbart'sche Verlagsbuchhandlung, Stuttgart, 175–18.

Kalantari K., Kananian A., Asiabanha A., Eliassi M. (2008) Source and tectonic setting of zarjebostan (NE OF Qazvin) Paleogene volcanic rocks using REE and HFSE elements. *Geosciences Scientific Quarterly Journal* 17: 140-149. DOI: https://doi.org/10.22071/gsj.2009.57853

Kamber B. S., Ewart A., Collerson K. D., Bruce M. C., McDonald G. D. (2002) Fluid-mobile trace element constraints on the role of slab melting and implications for Archaean crustal growth models. *Contributions to Mineralogy and Petrology* 144: 38-56. DOI: https://doi.org/ 10.1007/s00410-002-0374-5

Kaz'min V., Tikhonova N. (2006) Late Cretaceous-Eocene marginal seas in the Black Sea-Caspian region: paleotectonic reconstructions. *Geotectonics* 40: 169-182. DOI: https://doi.org/ 10.1134/S0016852106030022

Khodami M., Noghreyan M., Davoudian A. R. (2010) Geochemical constraints on the genesis of the volcanic rocks in the southeast of Isfahan area, Iran. *Arabian Journal of Geosciences* 3: 257-266. DOI: https://doi.org/ 10.1007/s12517-009-0053-1

Khosaravi M., Saadat S, Dabiri R. (2020) Evaluation of heavy metal contamination in soil and water resources around Taknar copper mine (NE Iran), *Iranian Journal of Earth Sciences* 12 (3), 212-222. DOI: https://doi.org/10.30495/ijes.2020.675578

Le Bas M. J., Lemaitre R. W., Streckeisen A., Zanettin B. (1986) A Chemical Classification of Volcanic-Rocks Based on the Total Alkali Silica Diagram. *Journal of Petrology* 27: 745-750. DOI: https://doi.org/10.1093/petrology/27.3.745

Le Roux P., Le Roex A., Schilling J. G., Shimizu N., Perkins W., Pearce N. (2002) Mantle heterogeneity beneath the southern Mid-Atlantic Ridge: trace element evidence for contamination of ambient asthenospheric mantle. *Earth and Planetary Science Letters* 203: 479-498. DOI: https://doi.org/10.1016/S0012-821X(02)00832-4

Liu S. A., Li S., He Y., Huang F. (2010) Geochemical contrasts between early Cretaceous ore-bearing and ore-barren high-Mg adakites in central-eastern China: implications for petrogenesis and Cu–Au mineralization. *Geochimica et Cosmochimica Acta* 74: 7160-7178. DOI: https://doi.org/10.1016/j.gca.2010.09.003

Macpherson C. G., Dreher S. T., Thirlwall M. F. (2006) Adakites without slab melting: high pressure differentiation of island arc magma, Mindanao, the Philippines. *Earth and Planetary Science Letters* 243: 581-593. DOI: https://doi.org/10.1016/j.epsl.2005.12.034

Martin H. (1999) Adakitic magmas: modern analogues of Archaean granitoids. *Lithos* 46: 411-429. DOI: https://doi.org/10.1016/S0024-4937(98)00076-0

Martin H., Smithies R., Rapp R., Moyen J. F., Champion D. (2005) An overview of adakite, tonalite–trondhjemite–granodiorite (TTG), and sanukitoid: relationships and some implications for crustal evolution. *Lithos* 79: 1-24. DOI: https://doi.org/10.1016/j.lithos.2004.04.048

McKenzie D., O'nions R. (1991) Partial melt distributions from inversion of rare earth element concentrations. *Journal of Petrology* 32: 1021-1091. DOI: https://doi.org/10.1093/petrology/32.5.1021

Moghazi A. K. M. (2003) Geochemistry of a Tertiary continental basalt suite, Red Sea coastal plain, Egypt: petrogenesis and characteristics of the mantle source region. *Geological magazine* 140: 11-24. DOI: https://doi.org/10.1017/S0016756802006994

Mollai H., Dabiri R., Torshizian H. A., Pe-Piper G., Wang W. E. (2021) Upper Neoproterozoic garnet-bearing granites in the Zeber-Kuh region from east central Iran micro plate: Implications for the magmatic evolution in the northern margin of Gondwanaland, *Geologica Carpathica* 72 (6): 461-81. DOI: https://doi.org/10.31577/GeolCarp.72.6.2

Moyen J. F. (2009) High Sr/Y and La/Yb ratios: the meaning of the “adakitic signature”. Lithos 112): 556-574. DOI: https://doi.org/10.1016/j.lithos.2009.04.001

Müller D., Groves D. I., Müller D. (1995) Potassic igneous rocks and associated gold-copper mineralization (Vol. 56): *Springer*. DOI: https://doi.org/10.1007/978-3-319-23051-1

Nakamura N. (1974) Determination of REE, Ba, Fe, Mg, Na and K in carbonaceous and ordinary chondrites. *Geochimica et Cosmochimica Acta* 38: 757-775. DOI: https://doi.org/10.1016/0016-7037(74)90149-5

Nazari H., Salamati R. (1998) Geological map of Rudbar 1:100000, *Geological Survey of Iran*, Tehran.

Orozco-Esquivel T., Petrone C. M., Ferrari L., Tagami T., Manetti P. (2007) Geochemical and isotopic variability in lavas from the eastern Trans-Mexican Volcanic Belt: slab detachment in a subduction zone with varying dip. *Lithos* 93: 149-174. DOI: https://doi.org/10.1016/j.lithos.2006.06.006

Ousta S.h., Ashja-Ardalan A., Yazdi A., Dabiri R., Arian M.A. (2024) Petrogenesis and tectonic implications of Miocene dikes in the southeast of Bam (SE Iran): Constraints on the development of active continental margin, *Geopersia,* 14 (1): 89-111. DOI: https://doi.org/10.22059/geope.2023.364334.648729

Pearce J. A. (2005) Mantle preconditioning by melt extraction during flow: Theory and petrogenetic implications. *Journal of Petrology* 46: 973-997. DOI: https://doi.org/ 10.1093/ petrology/egi007

Pearce J. A., Harris N. B., Tindle A. G. (1984) Trace element discrimination diagrams for the tectonic interpretation of granitic rocks. *Journal of Petrology* 25: 956-983. DOI: https://doi.org/10.1093/petrology/25.4.956

Pearce J. A., Norry M. J. (1979) Petrogenetic implications of Ti, Zr, Y, and Nb variations in volcanic rocks. *Contributions to Mineralogy and Petrology* 69: 33-47. DOI: http://dx.doi.org/10.1007/BF00375192

Pearce, J. A. (1983) Role of the Sub-Continental Lithosphere in Magma Genesis at Active Continental Margins. In: Hawkesworth, C. J. and Norry, M.J., Eds., Continental Basalts and Mantle Xenoliths, Shiva Cheshire, UK, 230-249.

Pe-Piper G., Piper D. J., Matarangas D. (2002) Regional implications of geochemistry and style of emplacement of Miocene I-type diorite and granite, Delos, Cyclades, Greece. *Lithos* 60: 47-66. DOI: https://doi.org/10.1016/S0024-4937(01)00068-8

Prouteau G., Scaillet B., Pichavant M., Maury R. (1999) Fluid-present melting of ocean crust in subduction. *Geology* 27: 1111-1114. DOI: https://doi.org/10.1130/0091-7613(1999)027<1111:FPMOOC>2.3.CO;2

Rapp R. P., Watson E. B. (1995) Dehydration melting of metabasalt at 8–32 kbar: implications for continental growth and crust-mantle recycling. *Journal of Petrology* 36: 891-931. DOI: https://doi.org/10.1093/petrology/36.4.891

Rapp R., Shimizu N., Norman M., Applegate G. (1999) Reaction between slab-derived melts and peridotite in the mantle wedge: experimental constraints at 3.8 GPa. *Chemical geology* 160(4): 335-356. DOI: https://doi.org/10.1016/S0009-2541(99)00106-0

Rezania ye Komachaly M. (2021) Petrology and geochemistry of Eshkaverat granitoeid dome in eastern Guilan, Northern Iran. MS. Theses. *Islamic Azad University, Lahijan Branch*, 180 p.

Rezania ye Komachaly V., Salavati M., Moghimi kandelus A. (2022) Geochemistry and tectono-magmatic setting of OIT plutonic gabbros in Northern Iran: New evidence for the Oceanic Plume magmatism in the Southern Caspian Sea. *Arabian Journal of Geosciences* 15:1-24. DOI: https://doi.org/ 10.1007/s12517-021-09363-7

Salavati M., Kananian A., Noghreiian M. (2012) Geochemical characteristics of volcanic suite from the easthern Guilan province Ophiolite complex in North of Iran. *Journal of applied sciences* 12: 1-11. DOI: https://doi.org/ 10.3923/jas.2012.1.11

Salavati M., Kananian A., Noghreyan M. (2013) Geochemical characteristics of mafic and ultramafic plutonic rocks in southern Caspian Sea Ophiolite (Eastern Guilan). *Arabian Journal of Geosciences* 6: 4851-4858. DOI: https://doi.org/10.1007/s12517-012-0688-1

Salavati M., Kananian A., Soofi A. S., Zaeimnia F. (2009) Mineral chemistry of ultramafic rocks from the Southern Caspian Sea Ophiolite (Eastern Guilan): evidence for a high-pressure crystal fractionation. *Irananin Journal of Crystallography and Mineralogy* 17: 149-166.

Salehpour S., Arian M.A., Rad A.J., Zarei Sahamieh R., Yazdi A. (2025) Geochemistry and technomagmatic environment of Eocene volcanic rocks in Yuzbashi Chay region, west of Qazvin (Iran), Iranian Journal of Earth Sciences, 17(1): 1-13. DOI: https://doi.org/10.57647/j.ijes.2025.1701.04

Sarem M. N., Abedini M. V., Dabiri R., Ansari M. R. (2021) Geochemistry and petrogenesis of basic Paleogene volcanic rocks in Alamut region, Alborz mountain, north of Iran. *Earth Sciences Research Journal* 25: 237-245. DOI: https://doi.org/10.15446/esrj.v25n2.74025

Seghedi I., Downes H., Vaselli O., Szakács A., Balogh K., Pécskay Z. (2004) Post-collisional Tertiary–Quaternary mafic alkalic magmatism in the Carpathian–Pannonian region: a review. *Tectonophysics* 393: 43-62. DOI: https://doi.org/10.1016/J.TECTO.2004.07.051

Shahabpour J. (2007) Island-arc affinity of the Central Iranian Volcanic Belt. *Journal of Asian Earth Sciences* 30: 652–665. DOI: https://doi.org/10.1016/j.jseaes.2007.02.004

Shaw D. M. (1970) Trace element fractionation during anatexis. *Geochimica et Cosmochimica Acta* 34: 237-243. DOI: https://doi.org/10.1016/0016-7037(70)90009-8

Skjerlie K. P., Patino Douce A. E. (2002) The fluid-absent partial melting of a zoisite-bearing quartz eclogite from 1.0 to 3.2 GPa; Implications for melting in thickened continental crust and for subduction-zone processes. *Journal of Petrology* 43: 291-314. DOI: https://doi.org/10.1093/petrology/43.2.291

Sun S. S., McDonough W. F. (1989) Chemical and isotopic systematics of oceanic basalts: implications for mantle composition and processes. *Geological Society, London, Special Publications* 42: 313-345. DOI: https://doi.org/10.1144/GSL.SP.1989.042.01.19

Talebian Borojenie H, Sheykhzakariaei S.J., Dabiri R., Yazdi A. (2025) Petrogenesis and tectonic implications of Neoproterozoic to Cenozoic A-type granitoids in NW Iran: geochemical and tectonic constraints, *Iranian Journal of Earth Sciences*, 17(4): 1-19. DOI: https://doi.org/10.57647/j.ijes.2025.16894

Teimouri S. S., Ghasemi H., Asiabanha A. (2018) The role of crustal contamination and differentiation in the formation of the Eocene volcanic rocks in Jirande area (Northwest of Qazvin). *Petrological Journal* 9: 71-90. DOI: https://doi.org/ 10.22108/ijp.2017.82007.0

Temel A., Gündoğdu M. N., Gourgaud A. (1998) Petrological and geochemical characteristics of Cenozoic high-K calc-alkaline volcanism in Konya, Central Anatolia, Turkey. *Journal of volcanology and geothermal research* 85: 327-354. DOI: https://doi.org/10.1016/S0377-0273(98)00062-6

Temizel I., Arslan M. (2008) Petrology and geochemistry of Tertiary volcanic rocks from the İkizce (Ordu) area, NE Turkey: Implications for the evolution of the eastern Pontide paleo-magmatic arc. *Journal of Asian Earth Sciences* 31: 439-463. DOI: https://doi.org/10.1016/j.jseaes.2007.05.004

Thorkelson D. J., Breitsprecher K. (2005) Partial melting of slab window margins: genesis of adakitic and non-adakitic magmas. *Lithos* 79: 25-41. DOI: https://doi.org/10.1016/j.lithos.2004.04.049

Valizadeh M. V., Abdollahi H. R., Sadeghian M. (2008) Geological investigations of main intrusions of Central Iran. *Geosciences Scientific Quarterly Journal* 17: 182-197. DOI: https://doi.org/10.22071/gsj.2009.57829

Wang K., Plank T., Walker J. D., Smith E. I. (2002) A mantle melting profile across the Basin and Range, SW USA. *Journal of Geophysical Research: Solid Earth* 107: 5-21. DOI: https://doi.org/10.1029/2001JB000209

Wang Q., Wyman D. A., Xu J., Jian P., Zhao Z., Li C., He B. (2007) Early Cretaceous adakitic granites in the Northern Dabie Complex, central China: implications for partial melting and delamination of thickened lower crust. *Geochimica et Cosmochimica Acta* 71: 2609-2636. DOI: https://doi.org/10.1016/j.gca.2007.03.008

Wang Q., Wyman D. A., Xu J., Wan Y., Li C., Zi F., Zhao Z. (2008) Triassic Nb-enriched basalts, magnesian andesites, and adakites of the Qiangtang terrane (Central Tibet): evidence for metasomatism by slab-derived melts in the mantle wedge. *Contributions to Mineralogy and Petrology* 155: 473-490. DOI: https://doi.org/10.1007/s00410-007-0253-1

Whitney D. L. and Evans B. W. (2010) Abbreviations for names of rock-forming minerals. *American Mineralogist* 95:185–187. DOI: https://doi.org/ 10.2138/am.2010.3371

Willson M. (1989) Igneous petrogenesis. A global tectonic approach. *Springer Netherlands*. DOI: https://doi. org/10.1007/978-1-4020-6788-4

Winter J. D. (2001) An introduction to igneous and metamorphic petrology. (No Title).

Xiao L., Zhang H., Clemens J., Wang Q., Kan Z., Wang K., Liu X. (2007) Late Triassic granitoids of the eastern margin of the Tibetan Plateau: Geochronology, petrogenesis and implications for tectonic evolution. *Lithos* 96: 436-452. DOI: https://doi.org/10.1016/j.lithos.2006.11.011

Xu J. F., Shinjo R., Defant M. J., Wang Q., Rapp R. P. (2002) Origin of Mesozoic adakitic intrusive rocks in the Ningzhen area of east China: partial melting of delaminated lower continental crust? *Geology* 30: 1111-1114. DOI: https://doi.org/ 10.1130/0091-7613(2002)030<1111:OOMAIR>2.0.CO;2

Yan J., Chen J. F., Xu X. S. (2008) Geochemistry of Cretaceous mafic rocks from the Lower Yangtze region, eastern China: Characteristics and evolution of the lithospheric mantle. *Journal of Asian Earth Sciences* 33: 177-193. DOI: https://doi.org/10.1016/j.jseaes.2007.11.002

Yang W., Li S. (2008) Geochronology and geochemistry of the Mesozoic volcanic rocks in Western Liaoning: Implications for lithospheric thinning of the North China Craton. *Lithos* 102: 88-117. DOI: https://doi.org/10.1016/j.lithos.2007.09.018

Zhai M., Fan Q., Zhang H., Sui J. (2007) Lower crustal processes leading to Mesozoic lithospheric thinning beneath eastern North China: underplating, replacement and delamination. *Lithos* 96: 36-54. DOI: https://doi.org/10.1016/j.lithos.2006.09.016

Zhang H. F., Parrish R., Zhang L., Xu W. C., Yuan H. L., Gao S., Crowley Q. G. (2007) A-type granite and adakitic magmatism association in Songpan–Garze fold belt, eastern Tibetan Plateau:

implication for lithospheric delamination. *Lithos* 97: 323-335. DOI: http://doi. org/10.1016/j. lithos.2007.01.002

Zhang K. J. (2014) Genesis of the Late Mesozoic Great Xing'an range Large Igneous Province in eastern central Asia: a Mongol–Okhotsk slab window model. *International Geology Review* 56: 1557-1583. DOI: https://doi.org/10.1080/00206814.2014.946541

Zhu D., Pan G., Mo X., Liao Z., Jiang X., Wang L., Zhao Z. (2007) Petrogenesis of volcanic rocks in the Sangxiu Formation, central segment of Tethyan Himalaya: A probable example of plume–lithosphere interaction. *Journal of Asian Earth Sciences* 29: 320-335. DOI: https://doi.org/10.1016/J.JSEAES.2005.12.004